N65 15190
(ACCESSION NUMBER) (THRU)
74 1
(PAGES) (CODE)
CR 60252 21
(NASA CR OR TMX OR AD NUMBER) (CATEGORY)
FACILITY FORM 602

GPO PRICE $ _____

OTS PRICE(S) $ _____

Hard copy (HC) 3.00

Microfiche (MF) .75

[redacted] Doppler Control System, [redacted]
[redacted] Project
Model [redacted]

[redacted]

[redacted]

MISSILE & SPACE SYSTEMS DIVISION
DOUGLAS AIRCRAFT COMPANY, INC.
SANTA MONICA/CALIFORNIA

DOUGLAS

Coning Damper Control System Analysis
Rebound Project
Model No. DSV-5

MARCH 1962
DOUGLAS REPORT SM-41560

Prepared by:
M. J. ASZUG, D. W. GOLDBERG, C. F. HARDING and J. M. LUTZ
Space Guidance and Control

Prepared for the National Aeronautics
and Space Administration
Under Contract No. NAS5-1294

Approved by:

K. W. Kerr, Chief
Space Guidance and Control Sections

Approved by:

H. O. Loshe, Chief
Manned Space Systems Engineering

SPACE SYSTEMS ENGINEERING | MISSILE & SPACE SYSTEMS DIVISION
DOUGLAS AIRCRAFT COMPANY, INC.

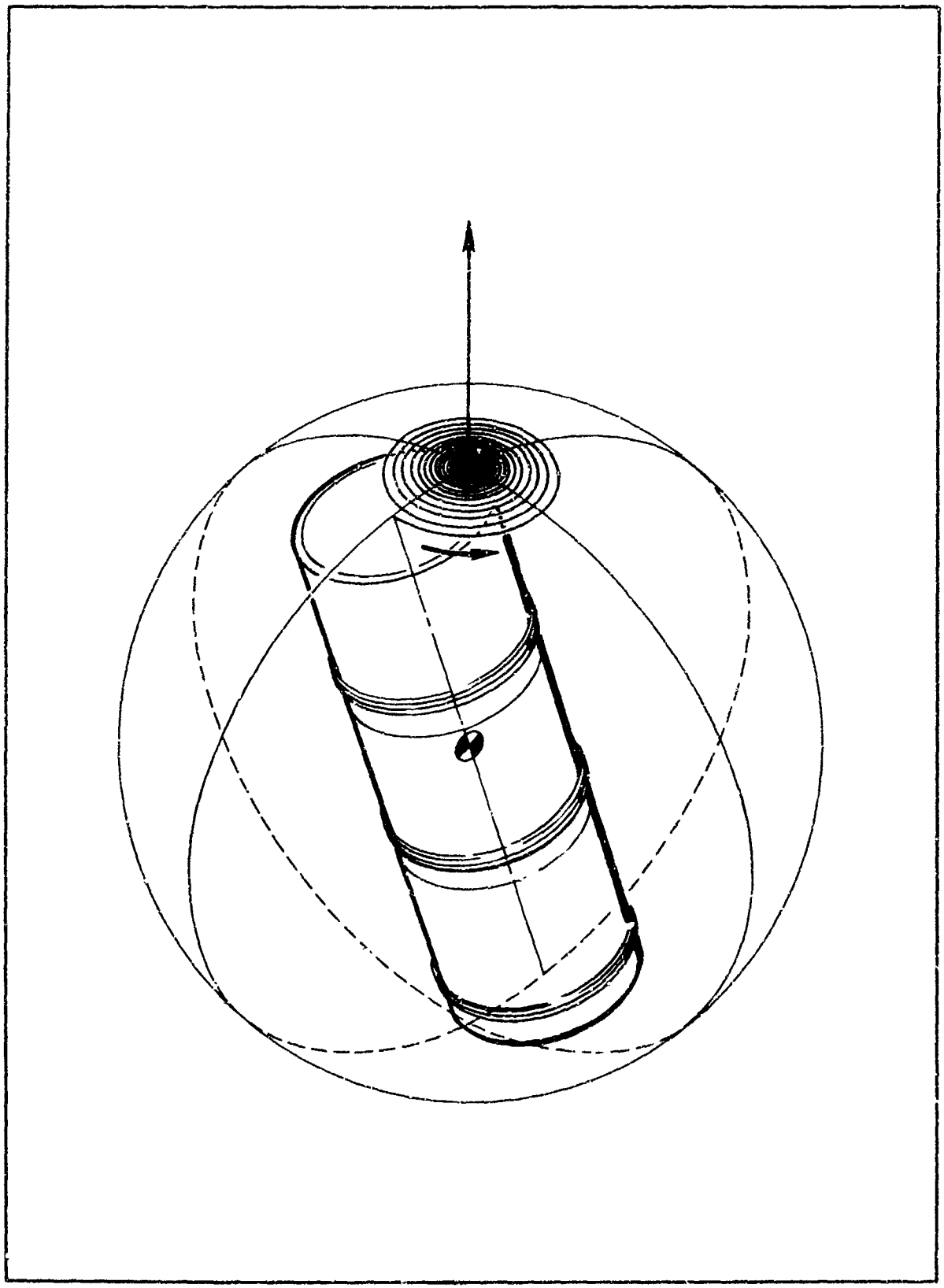

ABSTRACT

15190

The results of an analysis of a coning damper control system for the Rebound spacecraft is the subject of this report. The coning damper effectively maintains a desired spatial orientation of the spinning spacecraft. During coast periods it senses coning motion about the angular momentum vector and adds energy to the vehicle to overcome energy losses from internal vibration. It also reduces coning due to tipoff rates or any other coning angle sources.

Included in the report is an analysis of external disturbing influences affecting the vehicle spatial orientation. These disturbances are outside of the influence of the control system. A separate section of the report is devoted to an alternate control scheme employing an attitude gyro as the controller.

author

PREFACE

This report was prepared for the National Aeronautics and Space Administration as required on Contract NAS5-1294. The study was performed by the Guidance and Control Section of the Space Systems Engineering Division of Douglas Aircraft Company, Inc. The study period extended from January through March, 1962.

TABLE OF CONTENTS

Paragraph		Page
	SECTION 1 - INTRODUCTION	
	SECTION 2 - ANALYSIS OF EXTERNAL DISTURBANCES	3
2.	INTRODUCTION	3
2.1	External Torques on the Rebound Cannister Assembly	3
2.1.1	Gravitational, Magnetic, and Solar Radiation Effects	3
2.1.2	Separation System	7
2.2	Conclusions	8
	SECTION 3 - ANALYSIS OF CONING DAMPER	9
3.	GENERAL CONSIDERATIONS	9
3.1	System Description	9
3.1.1	Acceleration Block	9
3.1.2	Shaping Network	9
3.1.3	Motor Loop	13
3.1.4	Vehicle Dynamics	13
3.2	Linear Stability Analysis	13
3.2.1	Nyquist and Root Locus Analysis	15
3.2.2	Describing Function Analysis	21
3.3	Analog Simulation and Transient Response	21
3.3.1	Linear System Response	29
3.3.2	Torque Limited Response	29
3.4	Conclusions	29

TABLE OF CONTENTS (Continued)

Paragraph		Page
	SECTION 4 - CONING DAMPER USING CONTROL GYROS	35
4.	PRINCIPLE OF OPERATION	35
4.1	Derivation of the Control-Gyro Equations	35
4.1.1	Definition of Symbols	43
4.2	Conclusions Regarding the Control-Gyro Coning Damper	44
	SECTION 5 - GENERAL CONCLUSIONS	47
	APPENDIX I - SYSTEM EQUATIONS FOR THE CONING DAMPER USING A MOTOR FLYWHEEL	51
	APPENDIX II - MATHEMATICAL ANALYSIS OF THE EXTERNAL DISTURBANCES ON A SPIN-STABILIZED VEHICLE	57

LIST OF ILLUSTRATIONS

Figure		Page
1	Cumulative Angular Deviation (Magnetic Disturbances)	5
2	Cumulative Angular Deviation (Gravitational Disturbances)	6
3	System Block Diagram	10
4	Compensation Network	11
5	Compensation Network Frequency Response	12
6	Coordinate System for Coning Damper	14
7	Root Loci (Three Cannisters)	18
8	Root Loci (Two Cannisters)	19
9	Root Loci (One Cannister)	20
10	Nyquist Diagram (Three Cannisters)	22
11	Nyquist Diagram (Two Cannisters)	23
12	Nyquist Diagram (One Cannister)	24
13	Describing Function for Threshold (N_1)	25
14	Describing Function for Backlash (N_2)	26
15	Nyquist Diagram (Three Cannisters) Including Backlash and Threshold Describing Function	27
16	Transient Response to Initial Coning Angle with Tachometer Feedback	30
17	Transient Response to Initial Coning Angle without Tachometer Feedback	31
18	Transient Response to Initial Coning Angle (Torque Limited System)	32
19	Two Coning-Damper Arrangements Using Single-Gimbal control Gyros	36
20	Illustration of Body Axes for Rotor and Gimbal of Gyro Shown in Figure 19	37
21	Coordinate Systems for External Torques	60

LIST OF TABLES

Table		Page
1	Physical Parameters	16
2	System Gains and Constants	17

SECTION I

INTRODUCTION

1. The nature of the Rebound mission requires that the attitude of the spacecraft between injections of the cannister assemblies be very closely controlled. The present design of the Rebound system has assumed that the Agena-B, the second stage of the boost vehicle, remains attached to the spacecraft after burnout, and furnishes attitude control for the spacecraft in the transfer orbit. This stage uses a horizon scanner and a gyro compassing scheme for the attitude reference and uses a cold gas jet system for control. The present Agena-B would seriously degrade the spacecraft accuracy due to its inability to maintain the required attitude tolerances and the effect of energy added to the transfer orbit from its gas jet system.

An alternate approach toward meeting these system requirements on attitude and energy change is to spin the spacecraft and separate it from the Agena-B immediately after the transfer orbit has been attained. The cannister assemblies would then be individually separated and injected into the final orbit. This scheme would eliminate the problems of the Agena-B gas control system. The three spinup and despin sequences of the spacecraft would be replaced by the single spinup operation. The problem with such an approach for a long slender body is the degradation of the vehicle attitude by a coning motion caused by the loss of energy of the spinning body from internal flexing and damping. This phenomenon caused the attitude of Explorer I to degrade completely into a flat spin after approximately 10 hours in orbit. In order to solve this problem, the coning damper concept has been developed.

The coning damper is basically a very simple servo, relying on two concepts in its operation. First, the coning motion can be measured by an accelerometer placed on the periphery of the vehicle with its sensitive axis parallel with the design spin axis. The coning is registered as a sinusoidal output of the accelerometer. Second, energy can be transferred from a storage battery to the vehicle spin motion by proper actuation of internal masses and thereby the coning can be reduced. These two concepts furnish the two necessary elements for a control system; namely, a sensor and an actuator.

For the Rebound application the coning damper enjoys a fundamental advantage over a gas jet control system. As a result of the actuator being internal to the spacecraft, it cannot change the angular momentum of the vehicle or its rectilinear energy in the transfer orbit. With the exception of external torques on the vehicle, the angular momentum vector forms a gyro reference and is preserved until the injection of each of the three cannister assemblies. It is shown later in this report that the influences of the external moments on the vehicle during the long coast periods are negligible, and the change in angular momentum due to separation of each assembly is quite small.

The purpose of this report is to develop in detail the configuration and requirements of the servo components to be used in the coning damper and to demonstrate the practicability of the coning damper concept. In this first section an introduction and a general evaluation of the problem have been presented. The second section evaluates the effects of the various external disturbing influences, such as solar pressure and magnetic torque, and shows that they are well within allowable limits. The third section describes the detailed analysis of a coning damper using the axial torquing of a flywheel as the actuation scheme. In the fourth section there is presented a preliminary development of a damping system using the precession of a gyro as the actuation scheme. The relative merits of these various alternatives are also explained. Finally, in the fifth section a general discussion is given. This section is followed by an appendix which presents the system equations for the coning damper using a motor-flywheel and an appendix developing the equations for the external torques on the spacecraft.

SECTION 2
ANALYSIS OF EXTERNAL DISTURBANCES

2. INTRODUCTION

In order to consider the replacement of the Agena-B with a coning damper control system for attitude stabilization, the external disturbance effects, which are outside of the influence of the coning control system, must be evaluated. If the effects of external disturbances are small, only the coning damping action of the control system is required to maintain an accurate vehicle direction in space. The external torques caused by the vehicle's interaction with the Earth's gravitational and magnetic fields, vehicle exposure to solar radiation, and the unequal forces imparted by the separation springs, are evaluated in this section of the report. These torques cause displacement of the nominal angular momentum vector from the desired orientation. A detailed formulation and solution of the field effects is given in Appendix II.

2.1 External Torques on the Rebound Cannister Assembly

2.1.1 Gravitational, Magnetic, and Solar Radiation Effects

Formulae are given below for the deviation (magnitude) of the angular momentum vector as a function of time in circular orbit due to the vehicle's interaction with both the gravitational and magnetic fields. Solar pressure torques are extremely small and may be neglected. Figures 1 and 2 show the accumulated field effects on the different spacecraft configurations. The notation is as follows:

a	Magnetic field constant (2.0×10^{16} $\frac{\text{lb-ft}^2}{\text{amp}}$)
β	Orbital rate (rad-sec)
e	Fractional impulse error ratio of each separation spring
δ	Angular deviation (rad)
I_p	Pitch-yaw moment of inertia (slug-ft^2)

I_R	Roll moment of inertia (slug-ft^2)
ℓ	Lever arm of separation spring (ft)
m	Vehicle's magnetic dipole moment (amp-ft^2)
m_o	Mass of each cannister (slugs)
μ	Gravitational field constant ($1.4 \times 10^{16} \frac{ft^3}{sec^2}$)
M	Mass of remaining vehicle after separation (slugs)
R	Orbital radius (ft)
t	Time since spinup (sec)
T	Period of orbit (sec)
v	Relative spring-induced separation speed ($\frac{ft}{sec}$)
ϕ	Inclination of orbit (rad) (0 for equatorial orbits)
ω_1	Vehicle spin ($\frac{rad}{sec}$)

Gravitational Field

$$\delta_g \doteq \frac{3}{4} \left[\frac{\sqrt{\mu}}{\omega_1 R^{3/2}} \right] \frac{I_R}{I_P} \left| 1 - \frac{I_R}{I_P} \right| (\cos 2\beta t - 1) \tag{1}$$

Magnetic Field

$$\delta_m \doteq \frac{amt}{I_R \omega_1 R^3} \sqrt{\cos^2 \phi + \left[\frac{1}{2} \left(1 + \frac{3T}{4\pi t} \sin 2\beta t\right) \sin \phi \right]^2} \tag{2}$$

As can be seen from the above, δ_g varies sinusoidally (reaching a maximum and returning to zero twice per orbit) while δ_m approaches a linear function after an extended period of time. For the purposes of graphical representation, a composite of the different configurations has been prepared which gives the maximum possible deviation of the remaining satellite at any one point from an initial orientation of the system. It is assumed that the spacecraft remains in the 3-cannister configuration for 20 hours while the 2 and 1 cannister configurations can each orbit 3 or 8 times as

CUMMULATIVE ANGULAR DEVIATION (MAGNETIC DISTURBANCES)

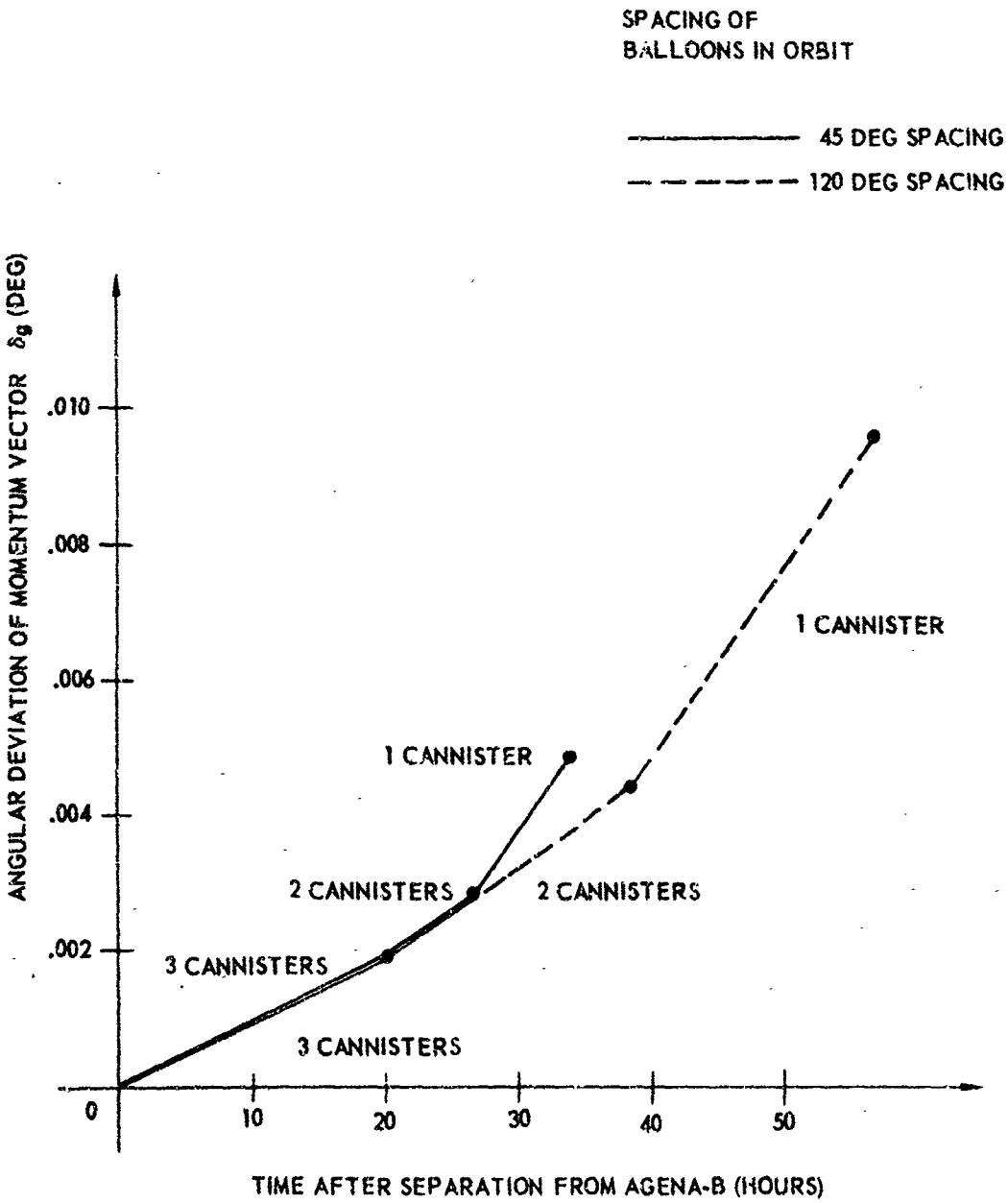

FIGURE 1

CUMMULATIVE ANGULAR DEVIATION (GRAVITATIONAL DISTURBANCES)

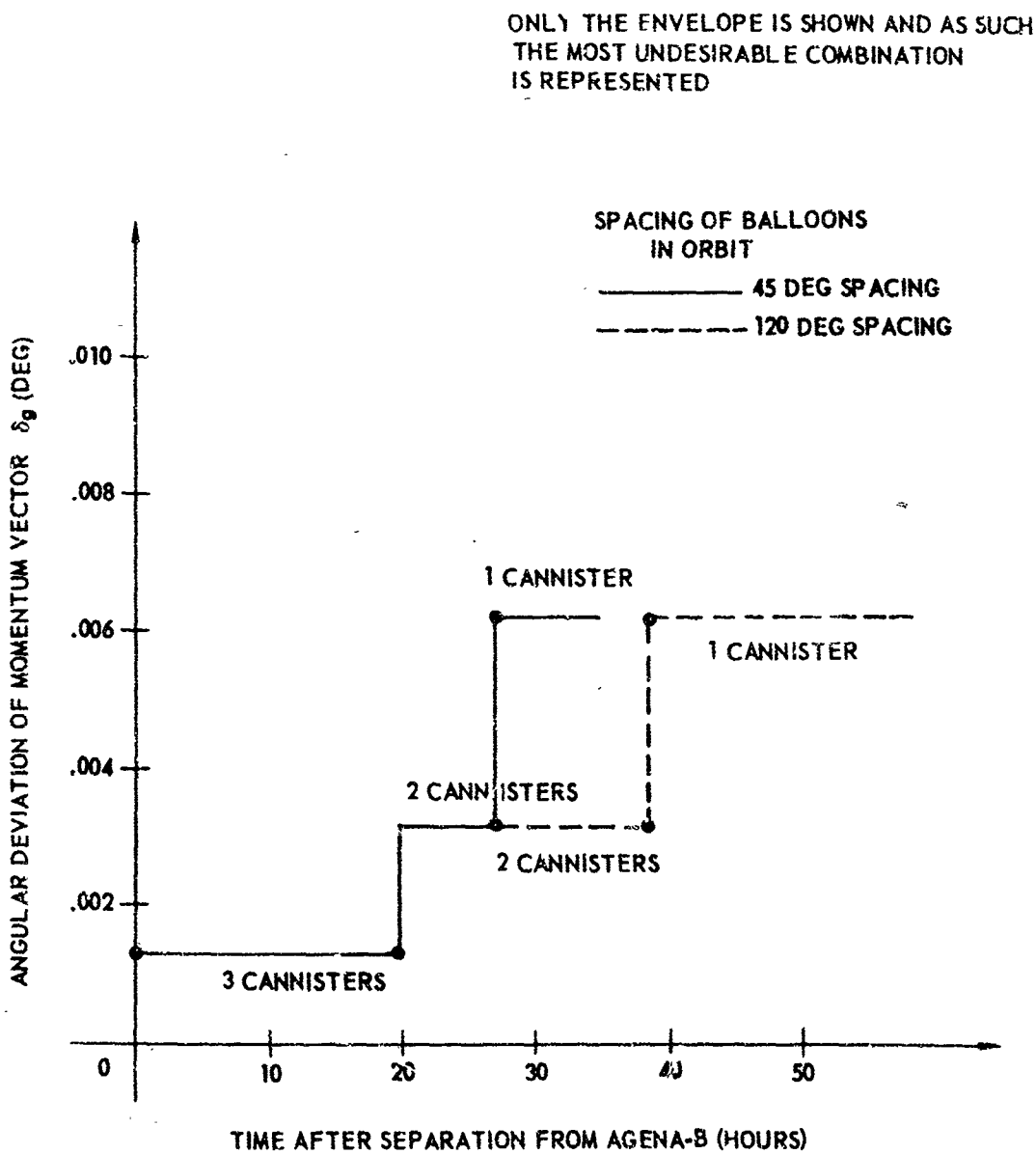

FIGURE 2

a unit, (spacings of 45° and 120°). An equatorial shot, $\phi = 0^\circ$, is given as the worst case (for magnetic effects), while the value of m has been chosen as 1/10 the value for Tiros II (this last is rather a pessimistic number for Rebound since the Tiros contains an additional dipole for attitude control purposes). A table is given below for the numerical values of the orbit and vehicle parameters.

	Number of Cannisters		
	1	2	3
$\beta = 7.58 \times 10^{-4}$ rad/sec			
$e = .61$			
$\ell = 2.0$ feet			
$m = 1$ amp-ft^2			
$m_o = 25.6$ slugs			
$R = 29.1 \times 10^6$ feet			
$t = (\text{sec} \times 10^{-4})$	10.52	8.86	7.20 (45° spacing)
	20.26	13.73	7.20 (120° spacing)
$T = 8.28 \times 10^3$ sec			
$N = 5.0$ ft/sec			
$\phi = 0$ rad			
$\omega_1 = 12.5$ rad/sec			

2.1.2 Separation System

The impulse unbalance of the spings used to eject the cannister assemblies from the spacecraft imposes an external impulse on the spacecraft angular momentum vector. This will alter the direction of the momentum vector by an amount

$$\sigma(\delta_i) = \frac{1}{2}\,\sigma(\bullet)\,\frac{v\ell}{i_R\,\omega_1}\left(\frac{Mm_o}{M+m_o}\right) \qquad (3)$$

For an impulse tolerance of 1% on each of the springs the three sigma value of the spacecraft attitude error is 0.136 deg, which is negligibly small.

The impulse uncertainty of the springs will cause an uncertainty in the backward velocity of the spacecraft due to the separation from a cannister assembly. Because the spacecraft is lighter without the Agene-B, it will have higher backward velocities with the coning damper scheme and will be more sensitive to impulse uncertainties. This backward velocity can be represented by

$$\sigma(v) = \frac{\sigma(\epsilon)}{2} \frac{m_o v}{(M+m_o)}$$

which in the present design would give a 3-sigma velocity error in the worst case of 0.0125 ft/sec, which is acceptable. This error can be decreased by reducing the separation velocity required or eliminated by turning on the velocity meters in the remaining cannister assemblies during the short period of time necessary to acrue this velocity change.

2.2 Conclusions

The external torques to which the Rebound system will be subjected have been investigated. These external torques are caused by the gravitational and magnetic fields of the earth, solar radiation pressure, and separation impulses. It was found that all these resulting errors are negligible except the backward-velocity effect on the spacecraft due to separation impulse and the resulting 3-sigma velocity error of 0.0125 ft/sec is acceptable. Also, this value can be reduced with minor redesign.

SECTION 3
ANALYSIS OF CONING DAMPER

3. GENERAL CONSIDERATIONS

The coning control system employs an accelerometer mounted on the periphery of the spinning spacecraft coupled with a motor flywheel system. The flywheel system is torqued by the motor in phase with the accelerometer output signal. The reaction torque on the spacecraft and the gyroscopically produced torque reduces the coning angle.

This section of the report describes in detail the analysis of the coning control system.

3.1 System Description

The block diagram of the Rebound coning control system used in this analysis is presented in Figure 3. The individual blocks of this diagram contain the various subsystem transfer functions and are described below.

3.1.1 Acceleration Block

The block ($F_{a\omega}$) in the diagram describes the dynamics of the accelerometer package relating output acceleration to the body angular rates. In this analysis the accelerometer instrument dynamics have been neglected since the natural frequency of the coning damper system is well below the natural frequency of existing accelerometers and the higher frequency accelerometer dynamic effects will be attenuated by lags in the system.

3.1.2 Shaping Network

The shaping network block (FAa) contains the transfer function of the RC network used for compensation. It will be shown that a shaping network is not needed for system stability. The network is used primarily to block D.C. commands to the motor flywheel as a result of accelerometer misalignments and other undesirable system residual signals. The shaping network configuration is shown in Figure 4, and the frequency response of the network is presented in Figure 5.

FIGURE 3

SYSTEM BLOCK DIAGRAM

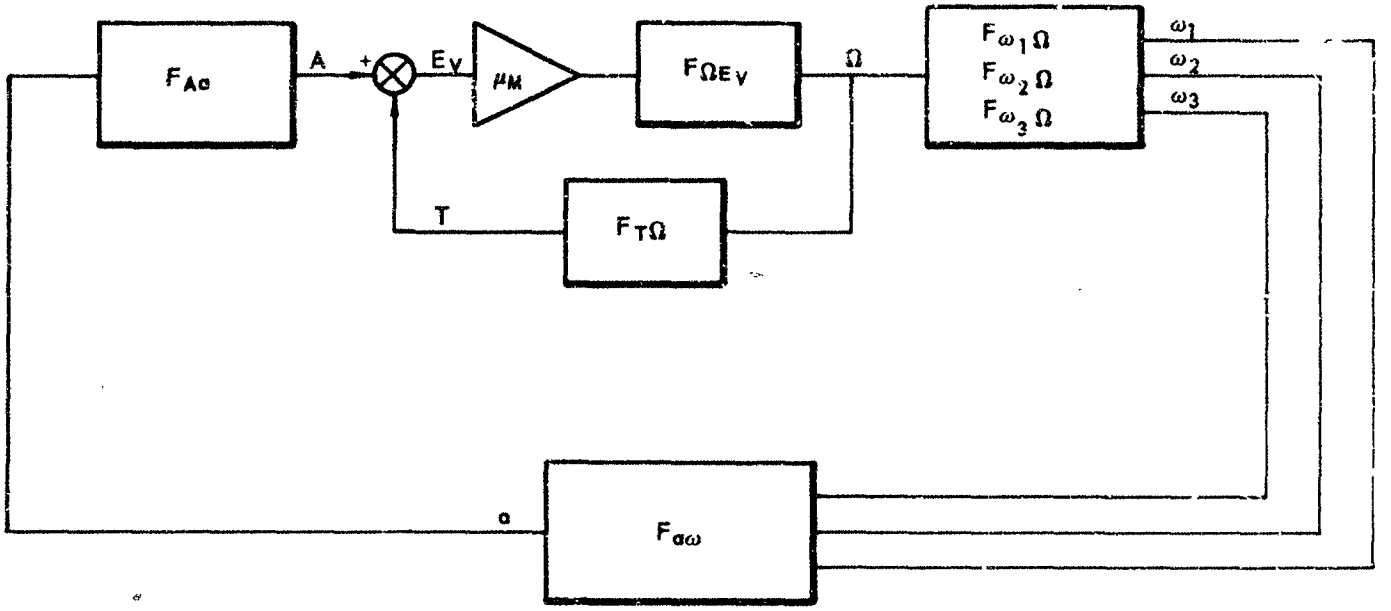

α – MEASURED ACCELERATION
$\omega_1, \omega_2, \omega_3$ – BODY ANGULAR RATES
Ω – FLYWHEEL ANGULAR RATE
A – SHAPED ACCELERATION SIGNAL

$F_{A\alpha}$ – SHAPING NETWORK
μ_M – AMPLIFIER
$F_{\Omega E_V}$ – MOTOR-FLYWHEEL
$F_{\omega\Omega}$ – VEHICLE DYNAMICS
$F_{\alpha\omega}$ – ACCELERATION DYNAMICS
$F_{T\Omega}$ – TACHOMETER

COMPENSATION NETWORK

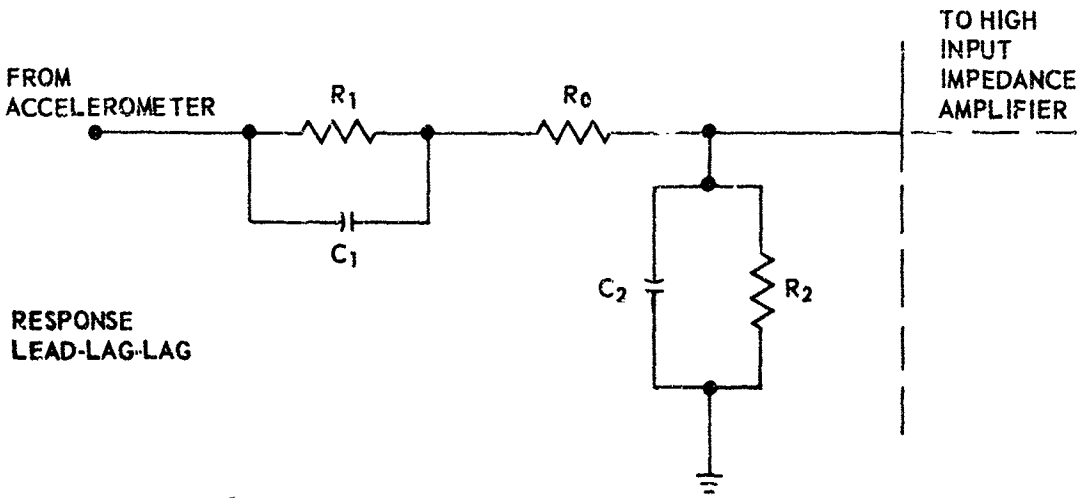

RESPONSE
LEAD-LAG-LAG

R_0 – 0.0887 MΩ
R_1 – 3.92 MΩ
R_2 – 0.100 MΩ

C_1 – 3.0 μf
C_2 – 0.10μf

TRANSFER FUNCTION

$$T.F. = \frac{\dfrac{R_2}{R_0 + R_1 + R_2}(1 + R_1 C_1 S)}{1 + \left[\dfrac{R_1 C_1 (R_0 + R_2) + R_2 C_2 (R_0 + R_1)}{R_0 + R_1 + R_2}\right] S + \left[\dfrac{R_0 R_1 C_1 R_2 C_2}{R_0 + R_1 + R_2}\right] S^2}$$

$$T.F. = \frac{0.020\,(1 + 11.72\,S)}{(1 + 0.3185S)\,(1 + 0.00796S^2)}$$

FIGURE 4

COMPENSATION NETWORK FREQUENCY RESPONSE

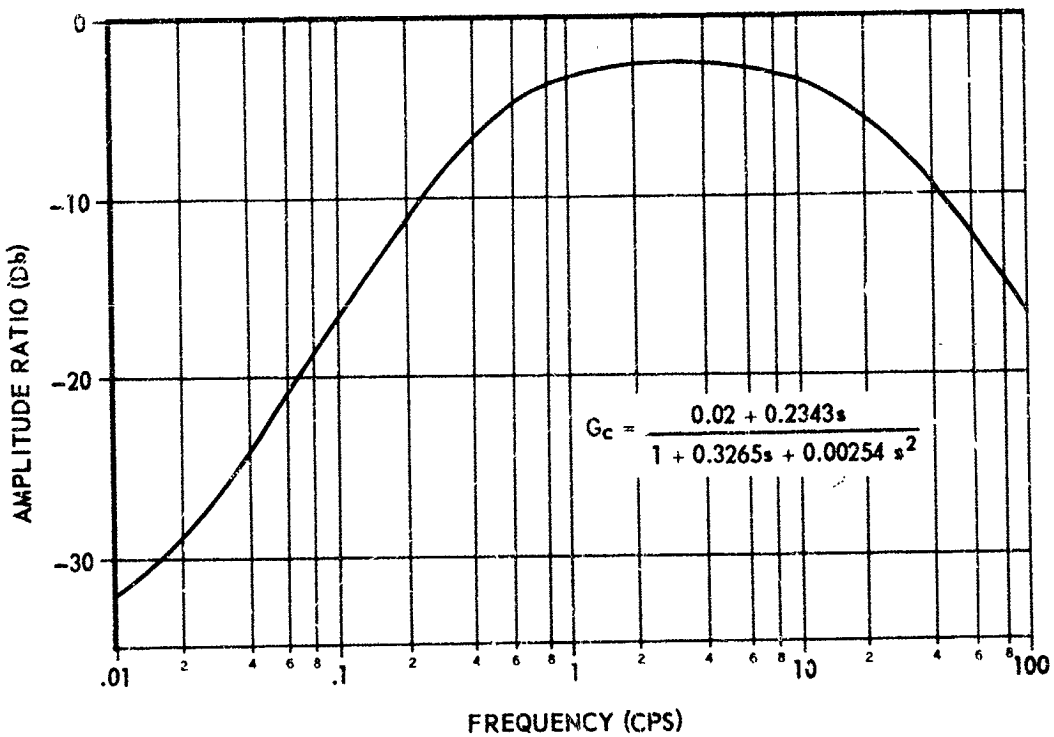

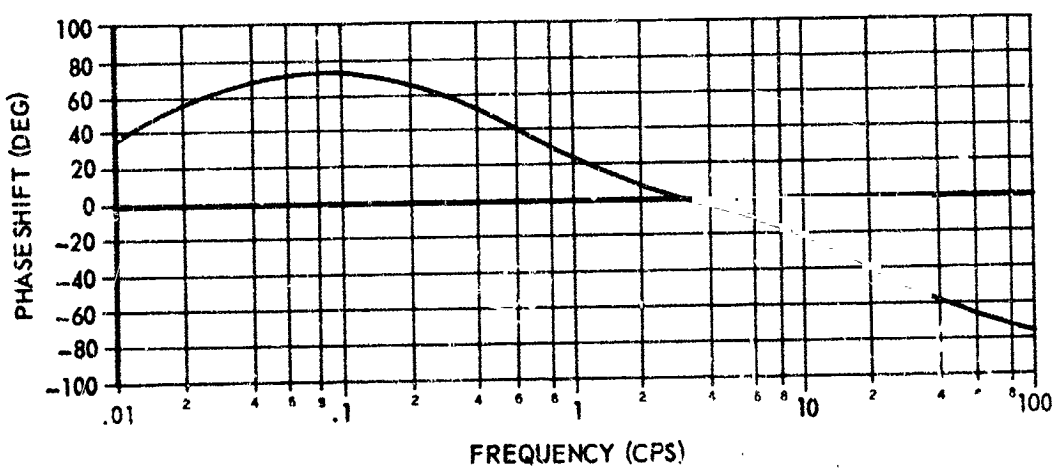

FIGURE 5

3.1.3 Motor-Loop

The block labeled motor loop represents the servo amplifier transfer function (μ_m), the transfer function of the servo motor, gear train and flywheel load ($F_\Omega F_V$), and the tachometer transfer function ($F_{T\Omega}$). The motor used is a relatively small size standard servo motor. A gear reduction between motor and load is used to obtain the proper torque-speed characteristic of the motor-flywheel necessary for desired system response. A relatively high gain amplifier is required to drive the motor, and since the motor is torque limited, the system behaves as a bang-bang controller. A tachometer to provide motor angular rate feedback has been included in the analysis only to determine its effect on system response. The actual system chosen does not include external rate feedback, and the tachometer will not be needed. Enough damping can be provided by the motor itself for the particular motor, flywheel, and gear ratio chosen.

3.1.4 Vehicle Dynamics

The dynamic block ($F_{\omega\Omega}$) contains the equations of motion relating the vehicle body angular rates to the flywheel speed. A description of the equations of motion are contained in Reference 2. These equations are also contained in Appendix I to this report. Here they are presented in a somewhat modified form which is more useful for controls analysis. The coordinate system is shown in Figure 6.

3.2 Linear Stability Analysis

System stability was investigated for the vehicle in three conditions, total vehicle (3 cannisters), 2 cannisters, and one cannister. Nyquist diagrams and root locus plots were obtained from an IBM 7090 digital computer program which solves the linearized control system and vehicle dynamic equations. Body torques on the flywheel have been neglected, as this is a second order effect. Several linearizing assumptions have been made in the vehicle dynamics to allow a linear approach to the analysis. These are described in Appendix I. Also, the effects of certain expected system non-linearities were determined using the describing function technique. The linear stability analysis was supported by an analog simulation of the complete equations. That analysis is described in Section 3.3.

COORDINATE SYSTEM FOR CONING DAMPER

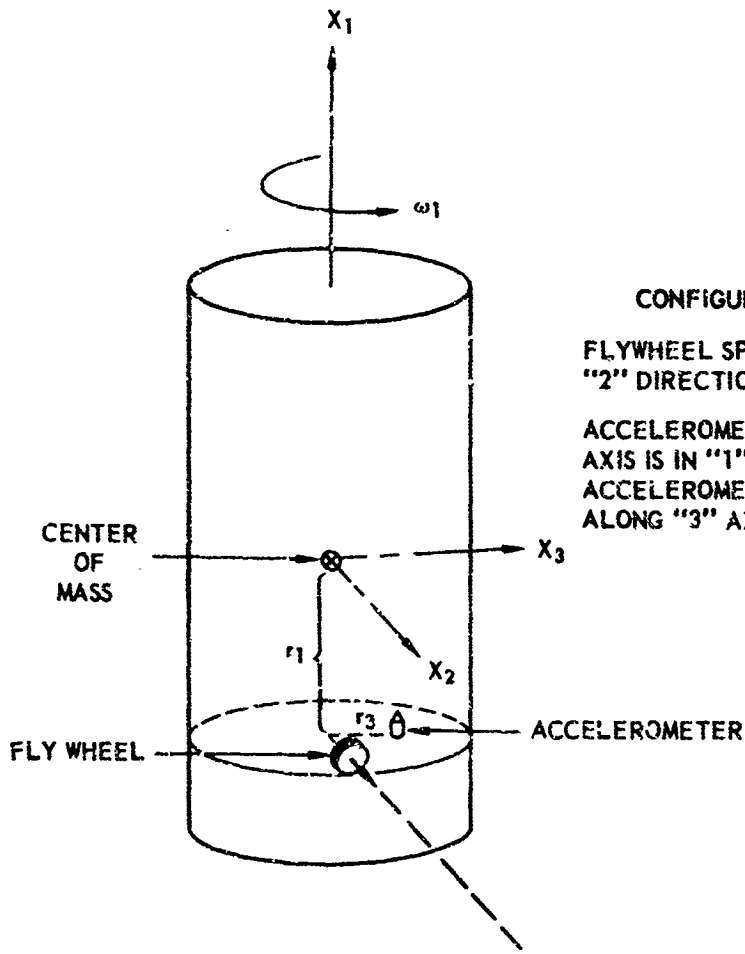

CONFIGURATION

FLYWHEEL SPIN AXIS IS IN "2" DIRECTION

ACCELEROMETER SENSITIVE AXIS IS IN "1" DIRECTION AND ACCELEROMETER IS MOUNTED ALONG "3" AXIS

3.2.1 Nyquist and Root Locus Analysis

The characteristic equation for the uncompensated control system is

$$1 + \frac{K_A K_M r_3 I_1}{I_p r_m} \, s \left[\frac{(s^2 + \omega_1^2)}{(s^2 + \lambda^2)(s + 1/r_m)} \right] = 0.$$

A typical Nyquist diagram can be closed, as shown below, to determine stability.

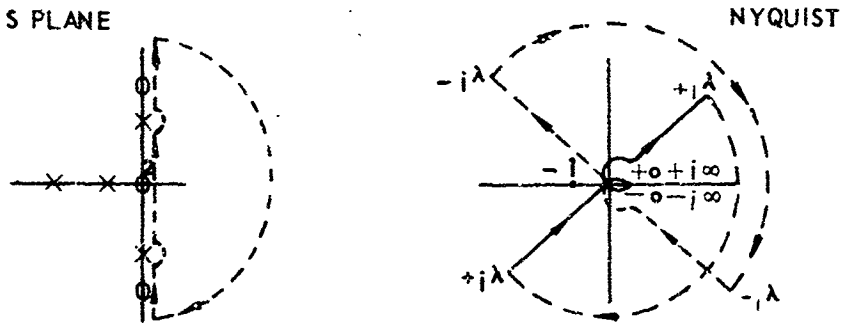

Since the system has no poles in the right half plane, no net encirclements of the minus one point are required for stability.

The various system parameters used in the analysis are as defined in Tables 1 and 2. Since $\lambda = \omega_{\perp} (1 - R)$ and $R = \frac{I_R}{I_p}$, λ will vary as the configuration changes from three cannisters to two cannisters and finally to one cannister. The root locus plots for the three different configurations are given in Figures 7 through 9. Notice that the poles due to the denominator term, $(s^2 + \lambda^2)$, move inward towards zero along the imaginary axis as first one and then the second cannister assembly is ejected. As a result of this change in λ, the root loci and hence the system roots will change for each of the three cases.

In analyzing the characteristic equation, digital computer programs were used in order to obtain the root locus plots and Nyquist diagrams for the system. As a result of making variations in the system parameters, it was found that a system loop gain of 1000 for a wheel moment of inertia of

TABLE I
PHYSICAL PARAMETERS

	VEHICLE		ACCELEROMETER LOCATION RADIUS				
	WEIGHT (LBS)	LENGTH (FT)	r_3 (FT)	I_R I_{ROLL} (SLUG-FT^2)	I_P I_{PITCH} (SLUG-FT^2)	I_1 I_{WHEEL} (SLUG-FT^2)	SPIN RATE ω_1 (RAD/SEC)
3 CANNISTERS	2475	12	2	141	658	0.05	12.5
2 CANNISTERS	1650	8	2	94	210	0.05	12.5
1 CANNISTER	825	4	2	47	35.5	0.05	12.5

$r_2 = .033$ FT

$R = I_R/I_P$

$\lambda = \omega_1 (1-R)$

TABLE II
SYSTEM GAINS AND CONSTANTS

SYMBOL	DESCRIPTION	VALUE		
		3 CANNISTERS	2 CANNISTERS	1 CANNISTER
$K_A K_M$	LOOP GAIN (RADIAN/SEC)/(FT/SEC/SEC)	1000	1000	1000
τ_m	MOTOR TIME CONSTANT (SECONDS)	0.5	0.5	0.5
R	RATIO OF VEHICLE ROLL TO PITCH INERTIA	.214	.447	1.325

ROOT LOCI (THREE CANNISTERS)

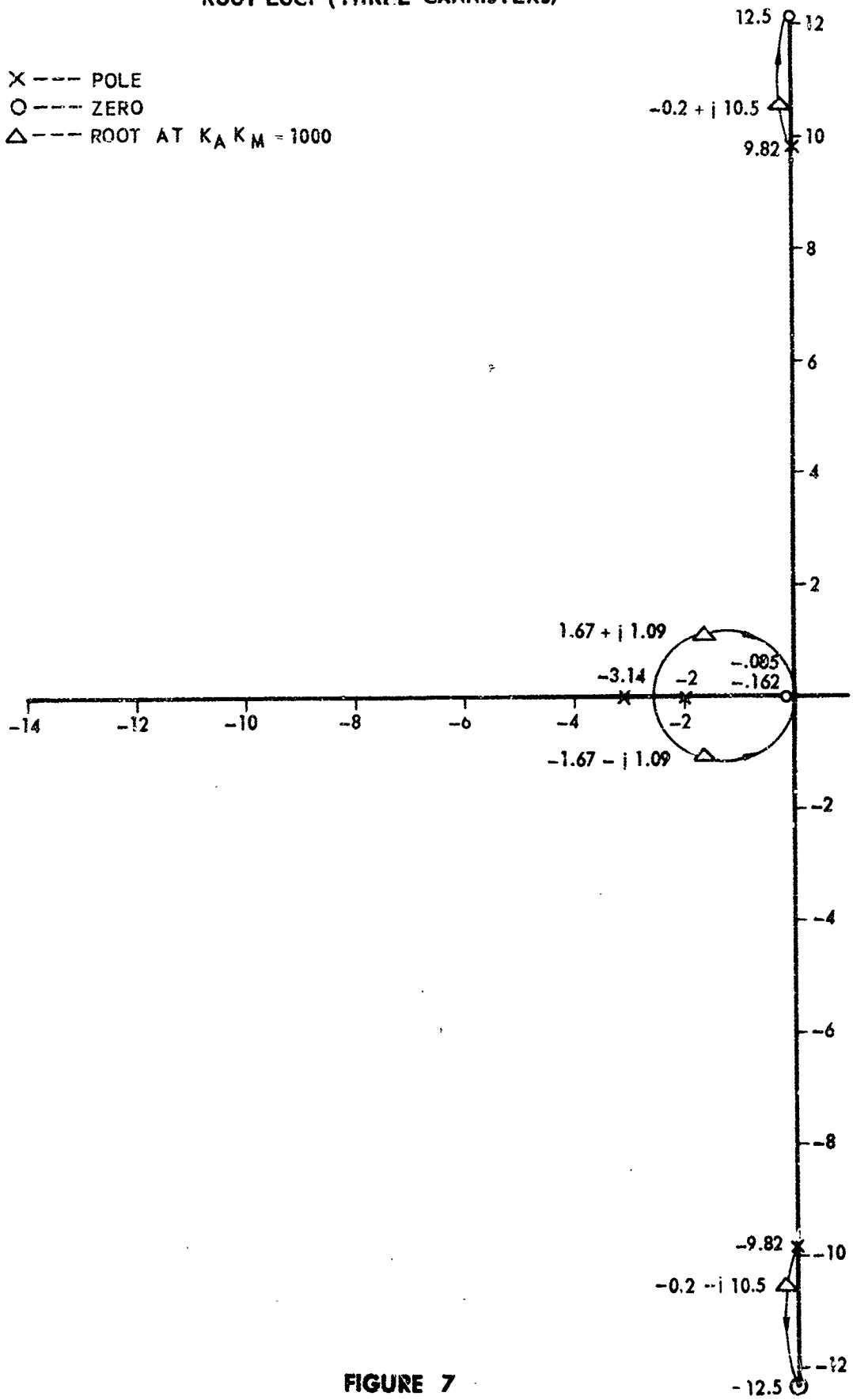

FIGURE 7

ROOT LOCI (TWO CANNISTERS)

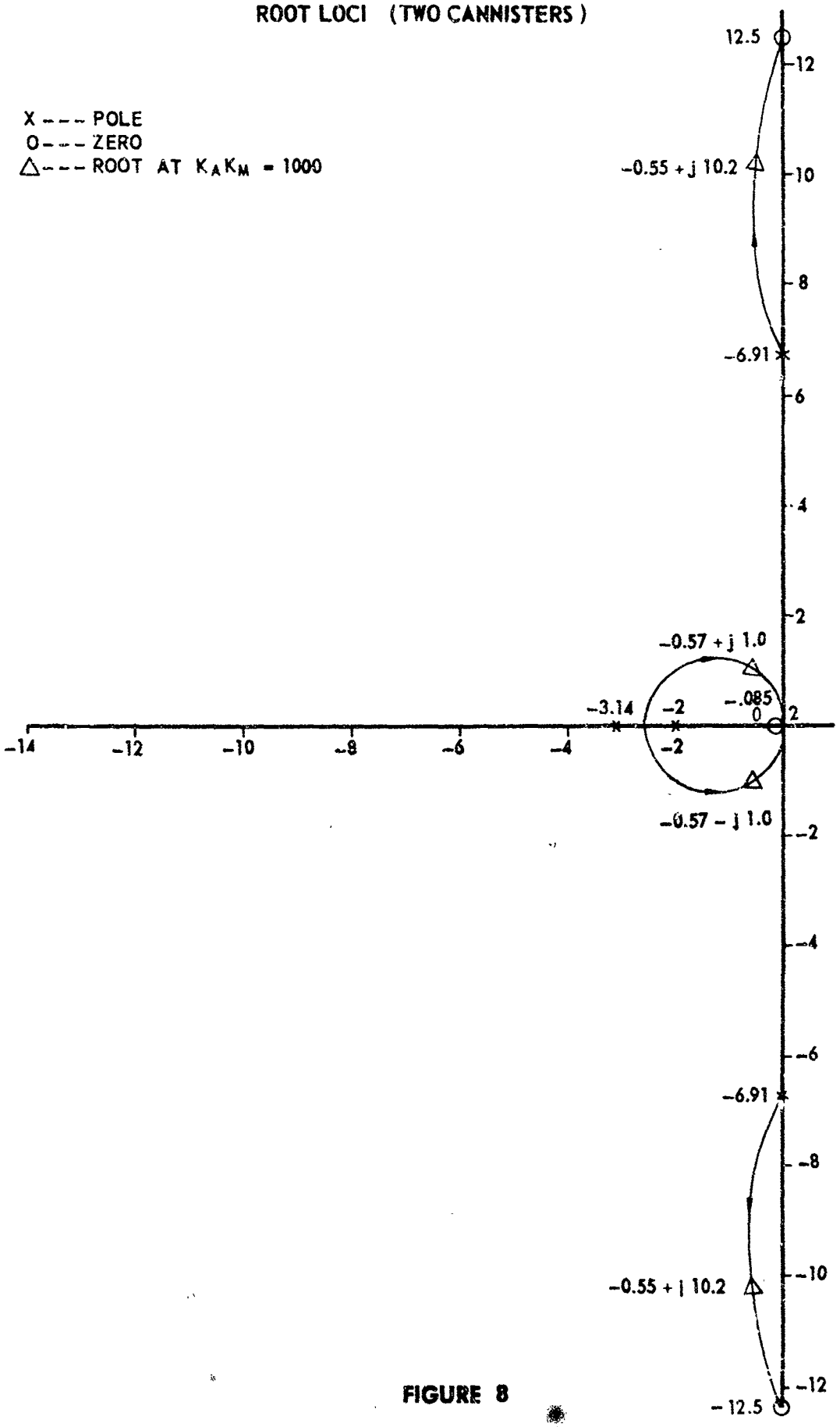

FIGURE 8

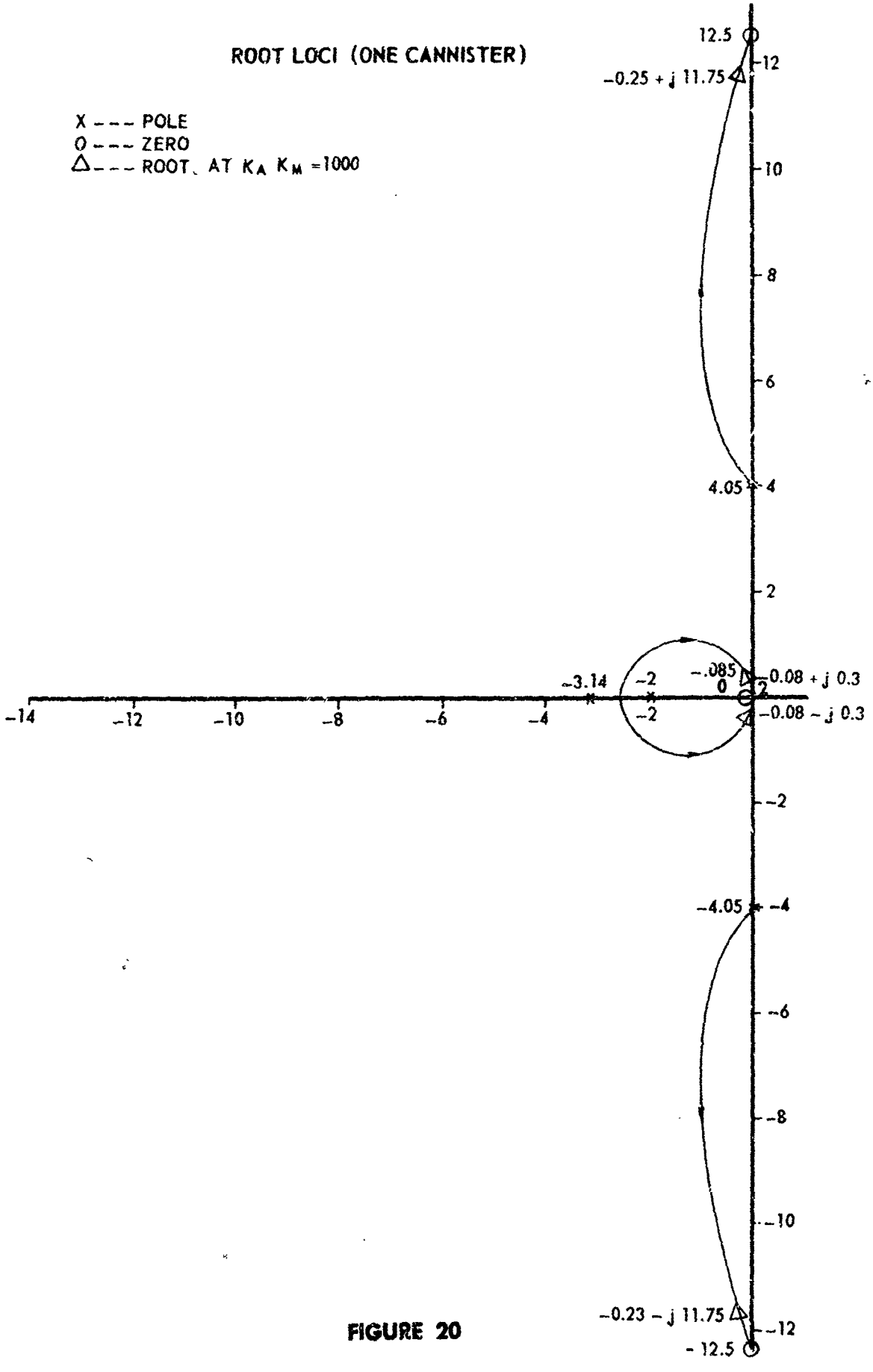
ROOT LOCI (ONE CANNISTER)
X --- POLE
O --- ZERO
△--- ROOT, AT $K_A K_M$ =1000
12.5
-0.25 + j 11.75
4.05
-.085
0
-3.14
-2
-2
0.08 + j 0.3
-0.08 - j 0.3
-4.05
-0.23 - j 11.75
- 12.5
-14
-12
-10
-8
-6
-4
12
10
8
6
4
2
-2
-4
-6
-8
-10
-12

FIGURE 20

0.05 slug-ft^2 provided good characteristics while at the same time being easily realizable. The system will remain stable for all values of gain provided that the accelerometer location along the r_2 axis is not greater than 0.033 ft. As r_2 approaches zero optimum response is achieved. Also, r_3 is to be made as large as possible so that the accelerometer is more sensitive to coning induced accelerations.

The Nyquist diagrams corresponding to the root loci plots are shown in Figures 10 through 12 for the various vehicle configurations. It can be seen that as the cannisters are ejected the system gain increases sharply. The system gain is proportional to I_1/I_p and as I_p decreases the loop gain increases. Even though the system gain increases drastically, the stability margins remain satisfactory.

3.2.2 Describing Function Analysis

The system can be expected to operate in a limit cycle manner since there will be a continual energy loss in the vehicle which must be overcome by the control system. Apart from this behavior, system dead bands, hysteresis and saturation may also cause either limit cycle or undesired response. Section 3.3 of this report contains a discussion of the analog simulation used to study the dynamic effects of saturation (torque limiting), showing that the system responds satisfactorily under this condition. To determine the effects of threshold and hysteresis with a linear analysis, the describing function technique was used. Since the system operates in a basically sinusoidal fashion, this technique can be expected to yield highly accurate results. Dead bands will be caused by thresholds in the accelerometer, in the servo amplifier and motor. Hysteresis or backlash is associated with the motor and gear train. Two describing functions were constructed. Figure 13 shows a typical describing function for dead band, figure 14 shows a describing function for backlash. These describing functions were used to construct the locus of "-1" points or amplitude characteristic on the linear Nyquist diagram, Figure 15. Since dead band alone introduces no phase shift into the system, this non-linearity has no effect on system response. For little or no energy loss in the vehicle, control will be applied until the signal amplitude falls within the deadzone at which time the control system ceases

NYQUIST DIAGRAM (THREE CANNISTERS)

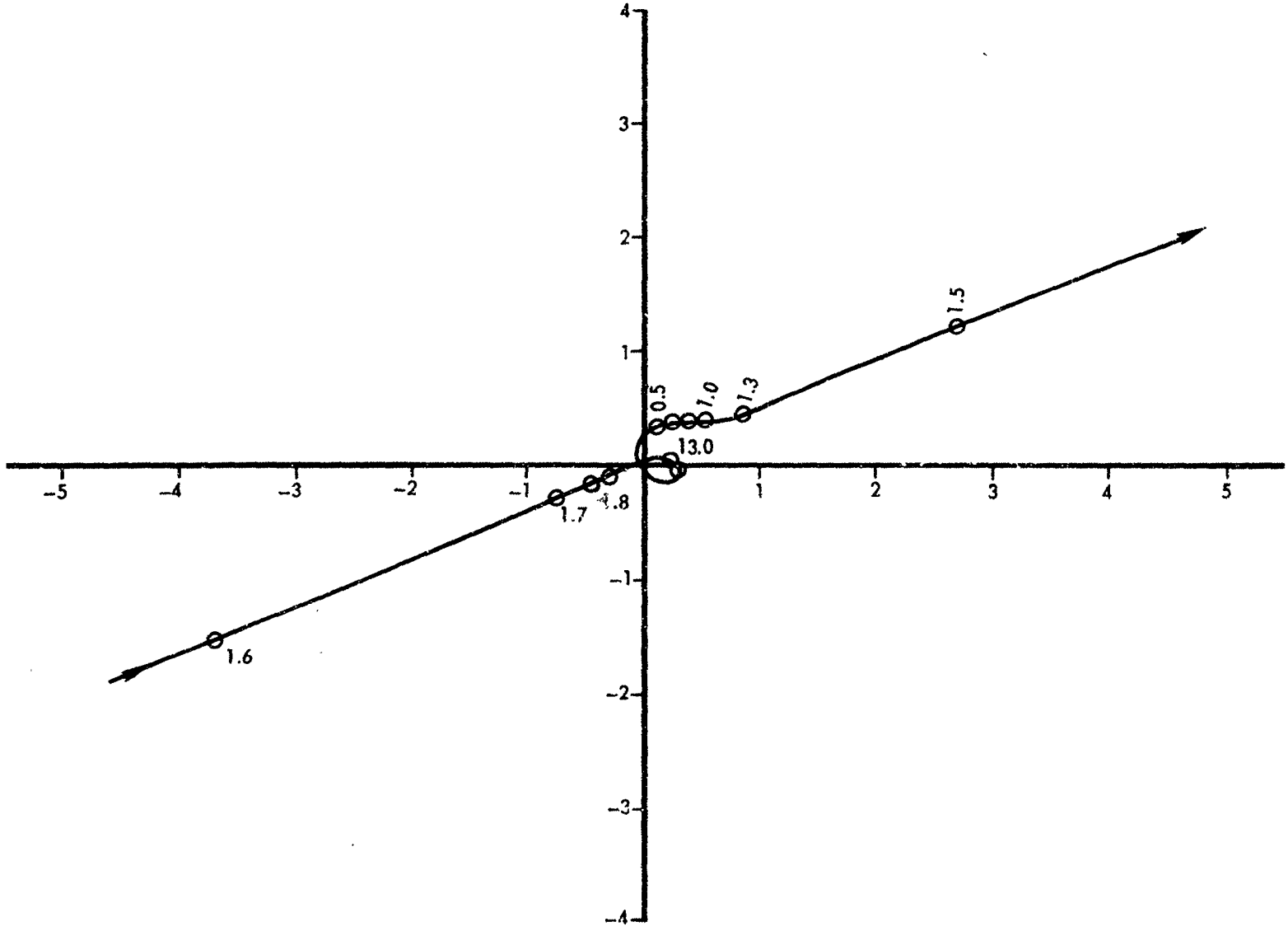

FIGURE 10

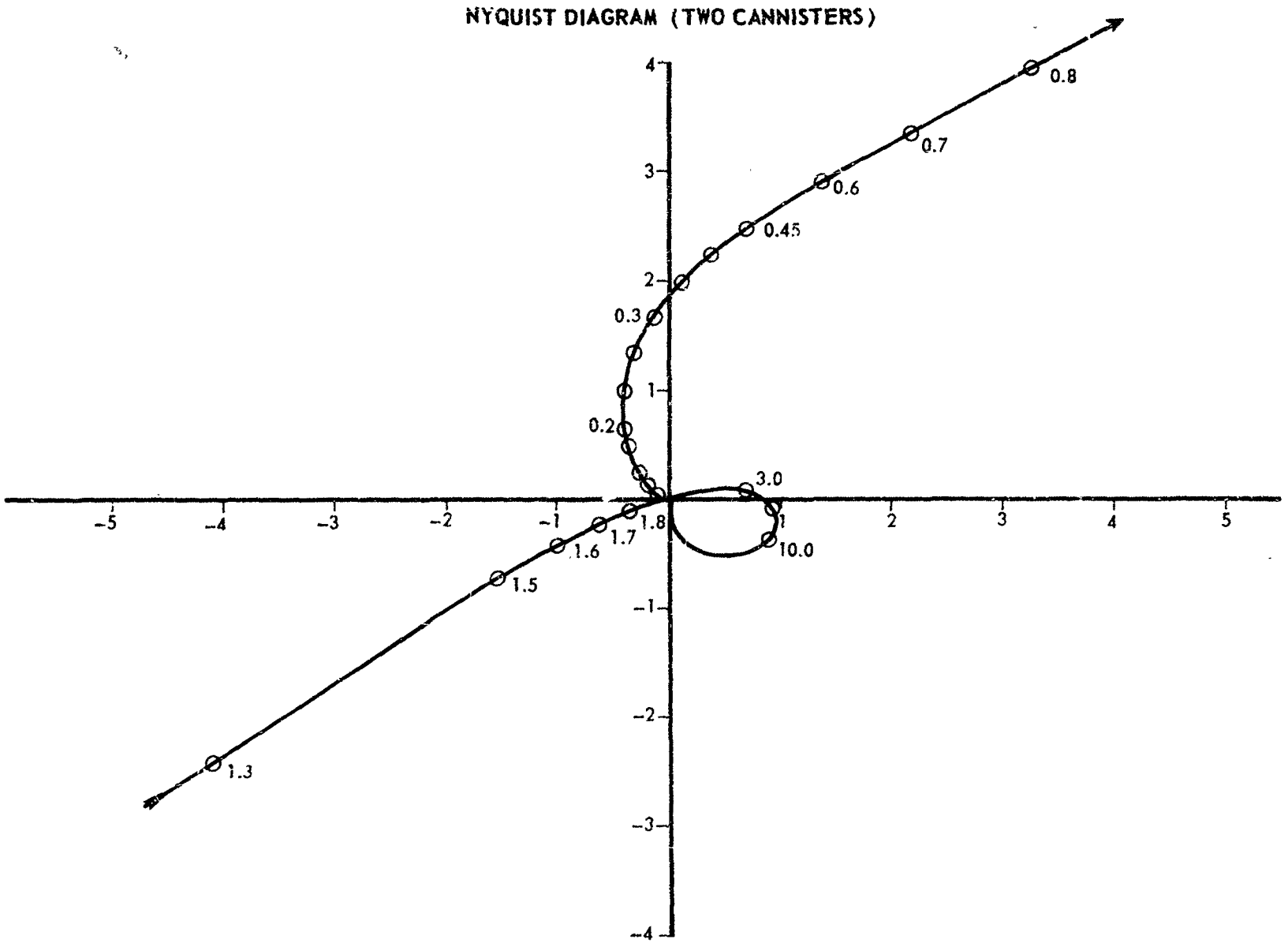
NYQUIST DIAGRAM (TWO CANNISTERS)
4
3
2
1
-1
-2
-3
-4
-5
-4
-3
-2
-1
1
2
3
4
5
0.8
0.7
0.6
0.45
0.3
0.2
3.0
1.8
1.7
1.6
1.5
1.3
10.0

FIGURE 11

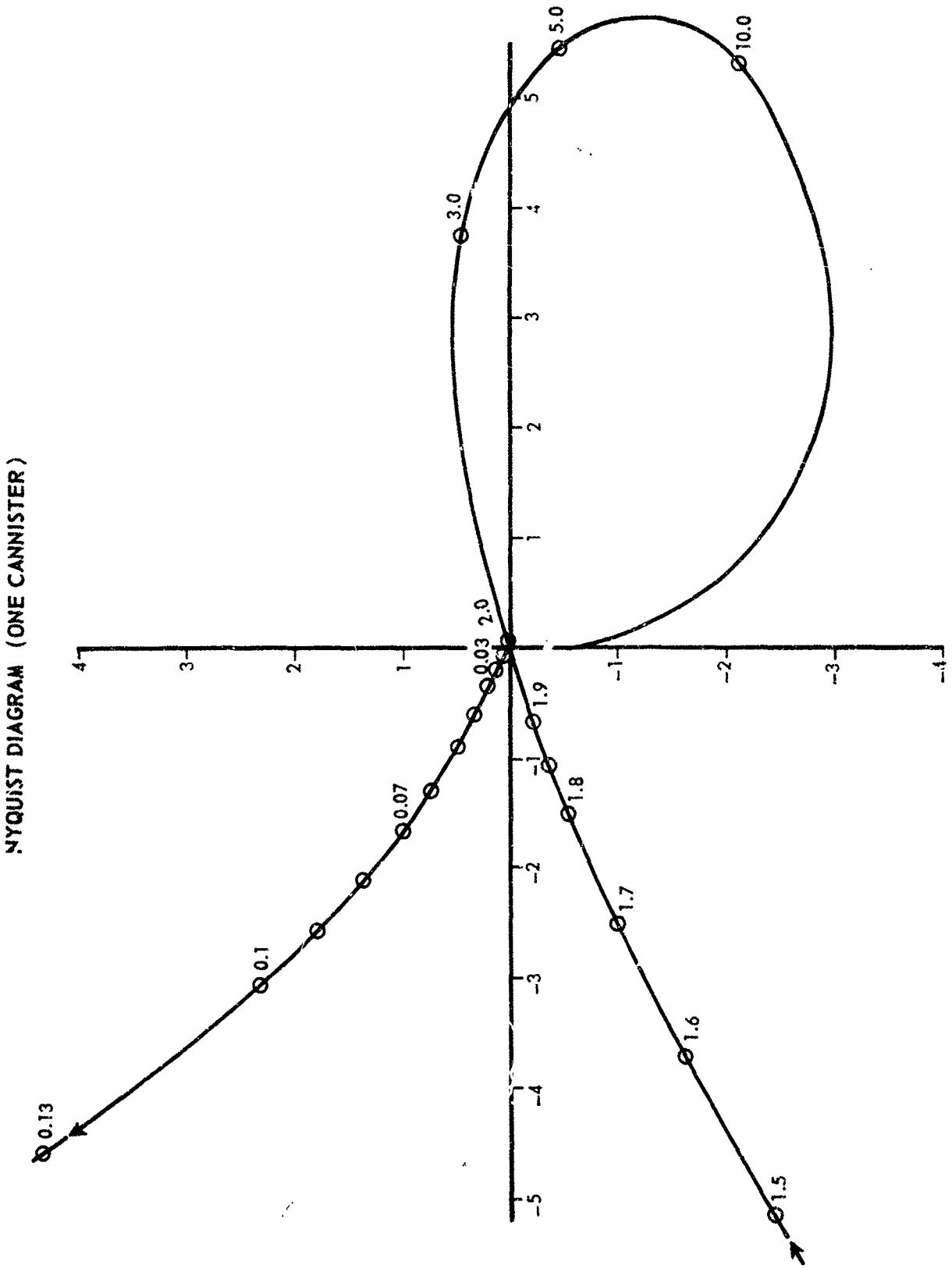
NYQUIST DIAGRAM (ONE CANNISTER)
0.13
0.1
0.07
0.03
2.0
1.9
1.8
1.7
1.6
1.5
3.0
5.0
10.0
4
3
2
1
-1
-2
-3
-4
-5
5
4
3
2
1
-1
-2
-3
-4

FIGURE 12

DESCRIBING FUNCTION FOR THRESHOLD (N_1)

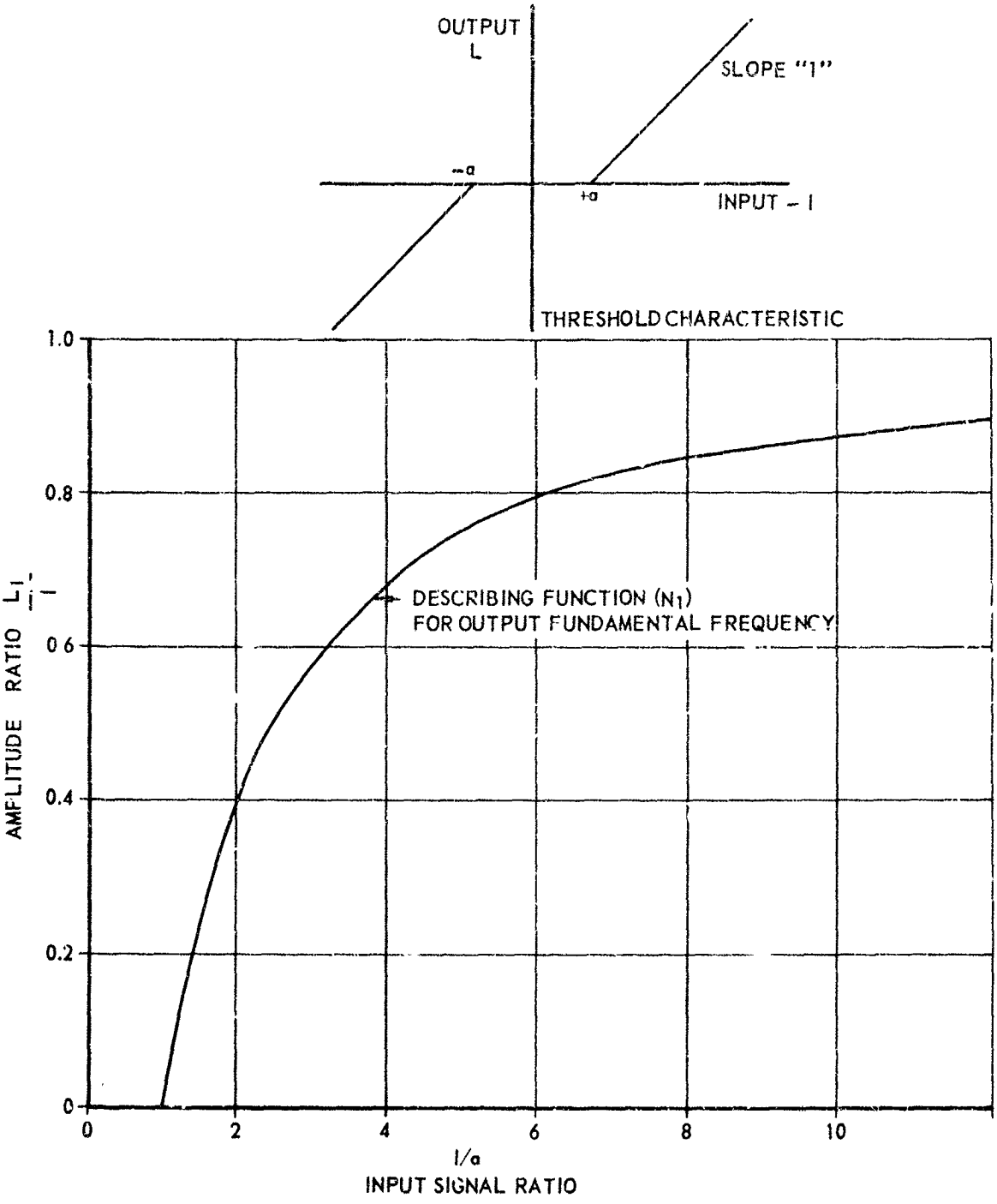

FIGURE 13

DESCRIBING FUNCTION FOR BACKLASH (N_2)

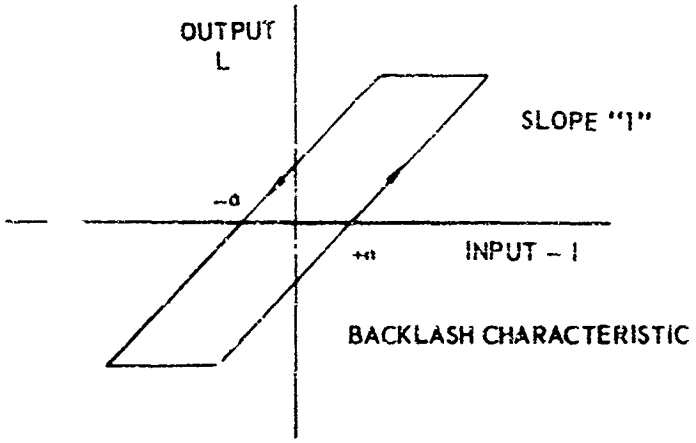

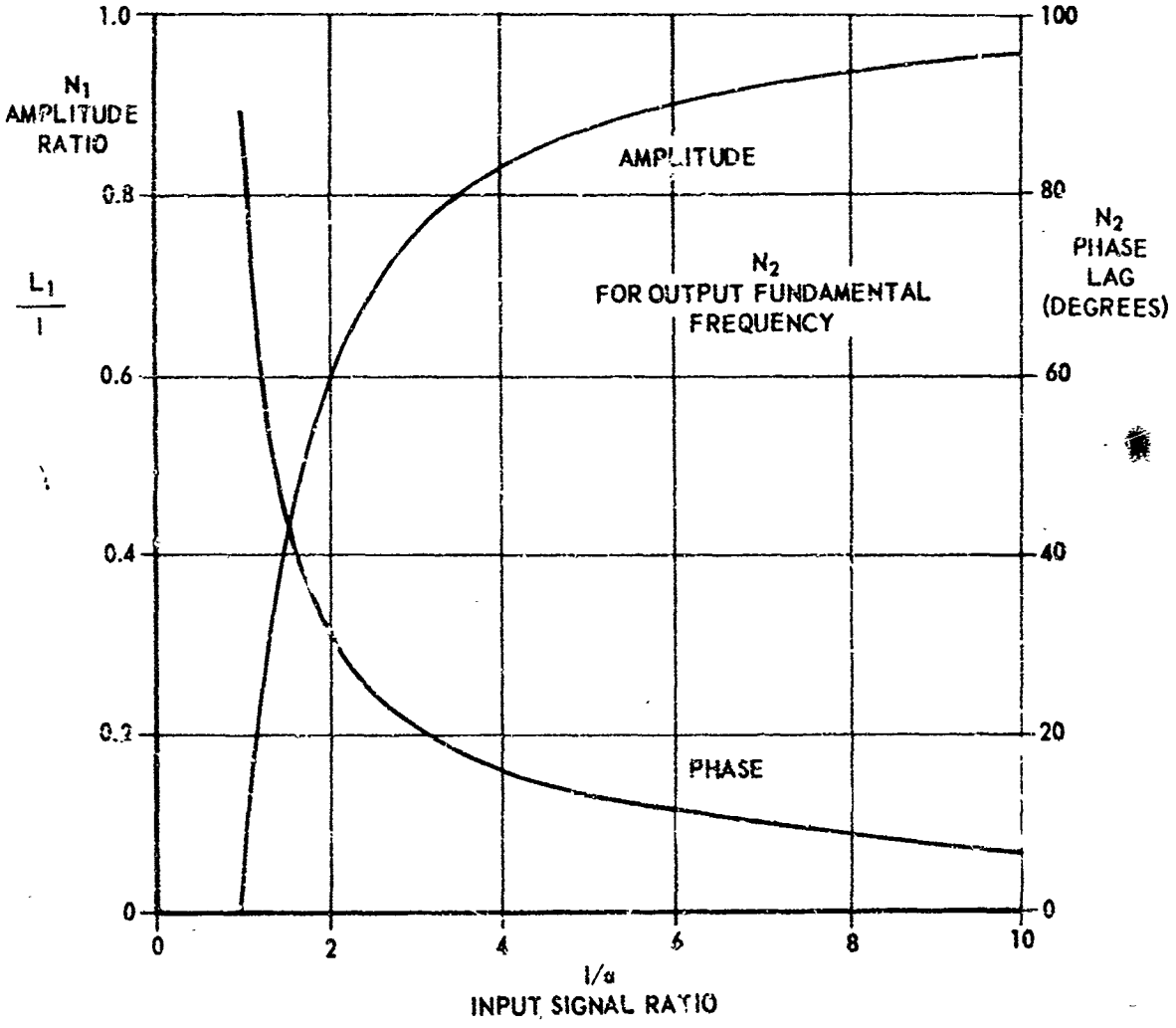

FIGURE 14

NYQUIST DIAGRAM (3 CANNISTERS)
INCLUDING BACKLASH AND THRESHOLD DESCRIBING FUNCTION

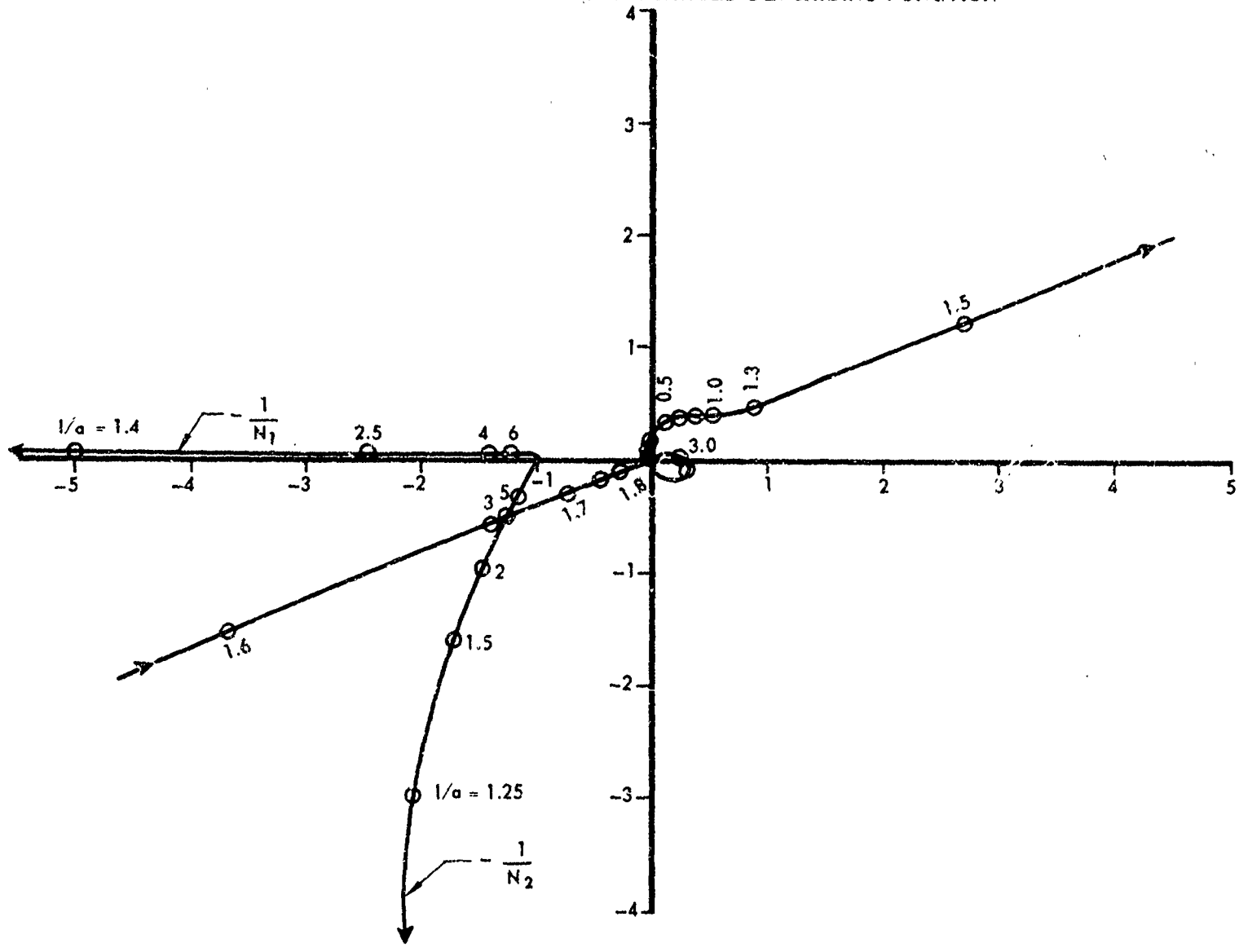

FIGURE 15

to respond. Here, the only requirement is that the amplitude of the dead zone be sufficiently small such that control is removed only when the coning angle is within acceptable limits. For example, in order to keep the coning angle within $\pm$ 0.1 degrees, the dead band of the accelerometer must be held within $\pm$ 0.228 ft/sec^2, which is well within the capability of existing low performance instruments. As a practical consideration it is possible to deliberately include a dead zone in the system equivalent to a small tolerable coning angle, insuring shutdown of the control system when not required and thus lowering power requirements.

In considering hysteresis or backlash, the additional phase lag introduced into the system by this effect can cause undesirable limit cycle operation. As seen in Figure 15 the amplitude characteristic function ($-1/N_2$) crosses the system frequency function. The frequency and amplitude at the crossover point indicate the limit cycle characteristics. However, it can be shown that the control system is relatively insensitive to backlash. In order to maintain the coning angle limit cycle amplitude within 0.1°, as much as 0.3 radians of gear train backlash at the flywheel can be tolerated. The gear train backlash can, of course, be easily kept much smaller than this value. Although the control system will be relatively unaffected by this non-linear condition, limit cycle amplitudes must be kept to small values for minimum power consumption. If required, further optimization of system parameters can improve the power consumption. For instance, additional phase lead can be added by the shaping network to decrease the limit cycle amplitude.

3.3 Analog Simulation and Transient Response

In order to evaluate the effects of system non-linearities neglected in the stability analysis and to size the motor-flywheel combination, an overall simulation of the control system was conducted with the aid of an analog computer. The exact equations of motion were mechanized including the effects of accelerometer positioning alignment errors.

3.3.1 Linear System Response

Figures 16 and 17 show system transient response for two different loop gains with and without tachometer feedback; it is seen that response can be made extremely rapid. However, for these systems impractically large motors are required to provide large torques and fast response. For the system of Figure 17 the peak angular acceleration required is equivalent to 7.5 ft-lbs of torque applied to a 0.05 slug-ft^2 inertia flywheel. For a larger wheel the required torque capability would be increased. These runs include the effects of small flywheel and accelerometer positioning and alignment errors. The misalignments had no detremental effect on system response. The most significant effect of accelerometer misalignment was the addition of a D.C. bias in the accelerometer signal. This D.C. bias was effectively removed by the high-pass shaping network.

3.3.2 Torque Limited Response

In order to size the control motor, various torque limits were mechanized in the analog simulation. The maximum torque capability was decreased until what was felt as minimum satisfactory response was achieved. Figure 18 shows the system response to an initial coning angle of 0.25° at a torque limit of 200 in-oz. Under these conditions the system drives the coning angle to 0.1° within 300 seconds and to zero with 500 seconds. The maximum required flywheel angular rate is 3.7 radians per second. These torque-speed characteristics can be easily obtained with a small motor, (10-20 watts), and the proper gear ratio reduction.

3.4 Conclusions

The results of the analysis of the motor flywheel control system have demonstrated that a satisfactory system can be obtained exhibiting adequate stability margins and response time.

A considerable variance of control system parameters have been studied. The control components assumed were deliberately kept conservative; yet, considerable freedom exists in the system for achieving an optimum design

TRANSIENT RESPONSE TO INITIAL CONING ANGLE
WITH TACHOMETER FEEDBACK
(ONLY THE ENVELOPE IS SHOWN)

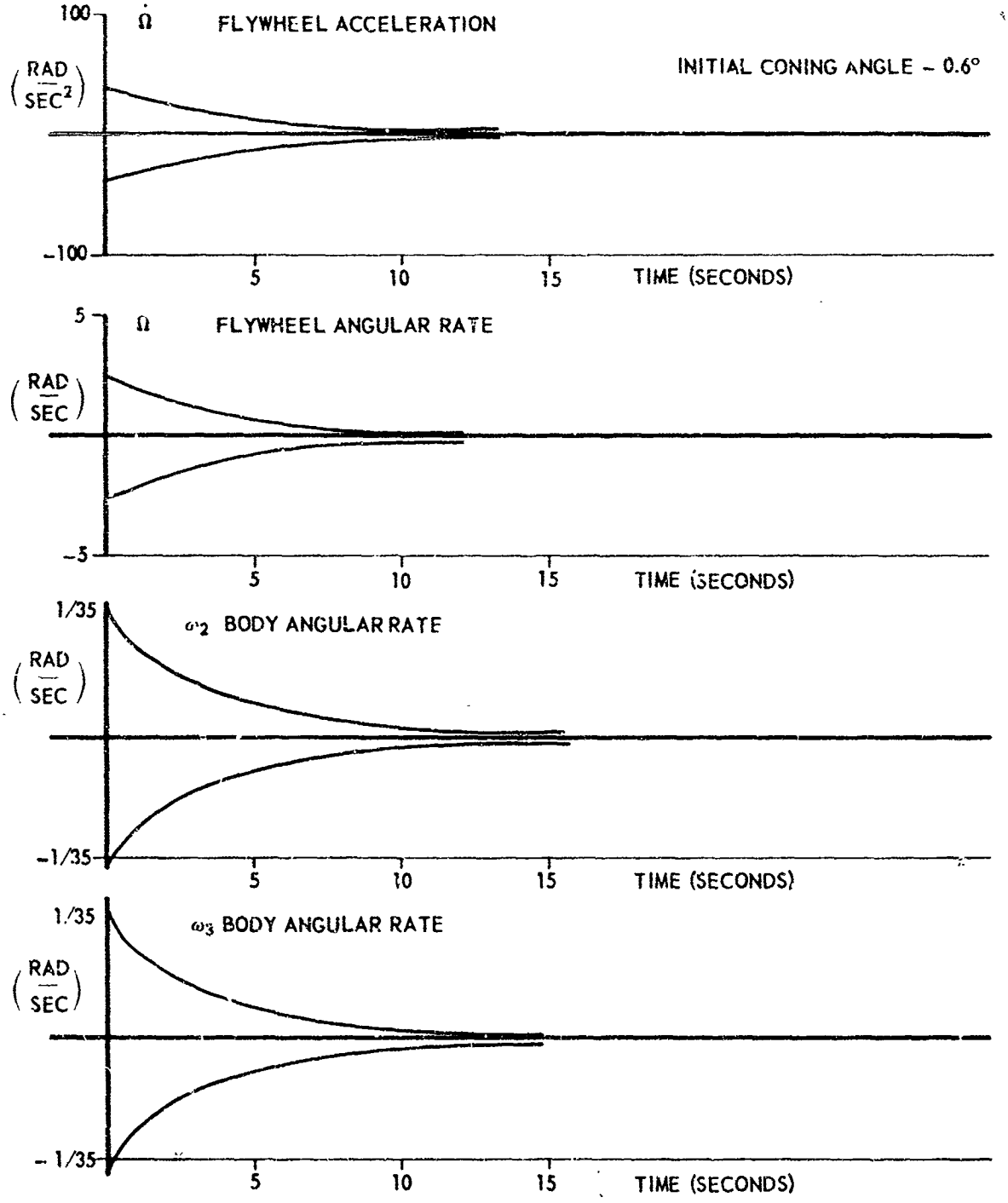

FIGURE 16

TRANSIENT RESPONSE TO INITIAL CONING ANGLE
WITHOUT TACHOMETER FEEDBACK
(ONLY THE ENVELOPE IS SHOWN)

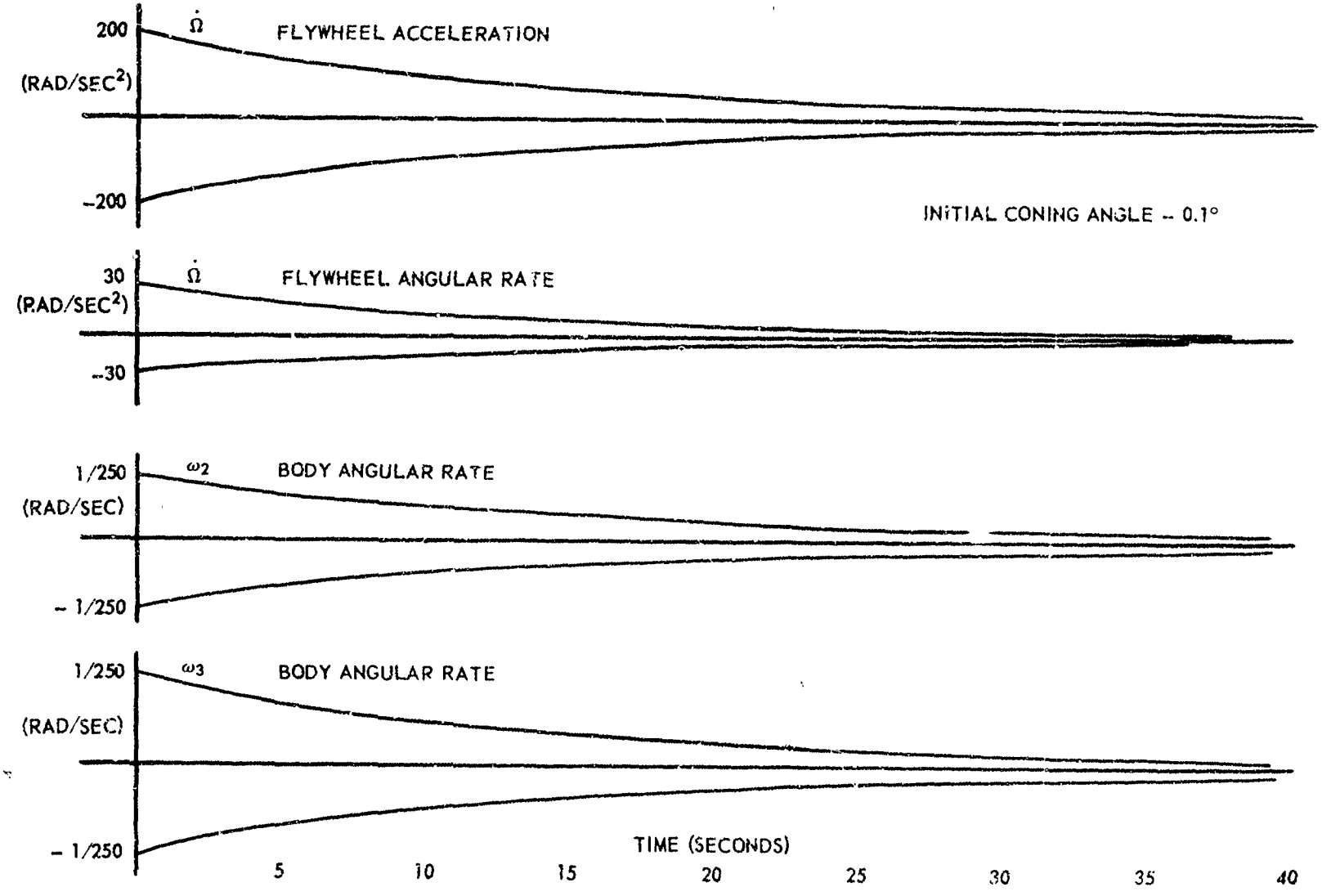

FIGURE 17

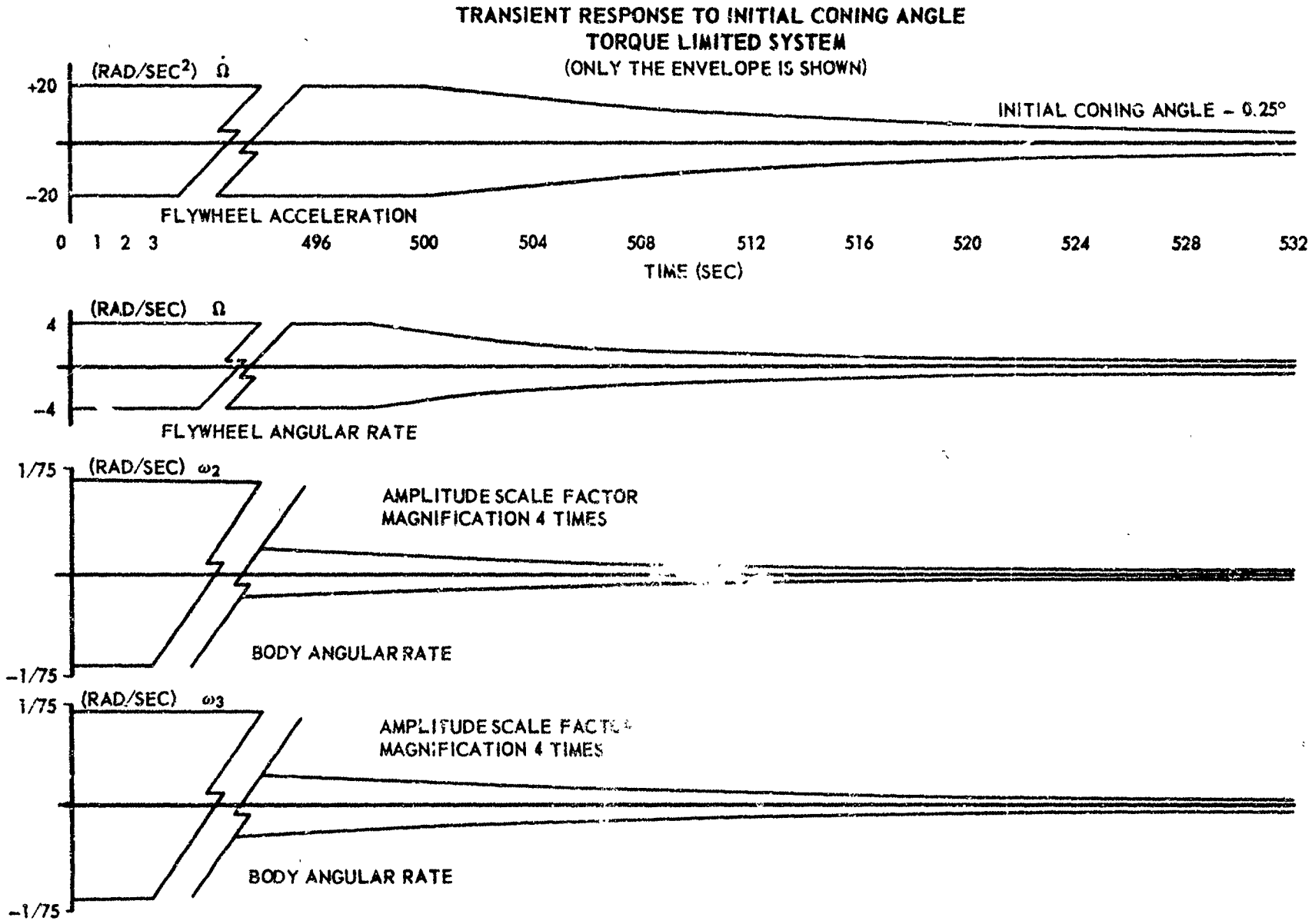
TRANSIENT RESPONSE TO INITIAL CONING ANGLE
TORQUE LIMITED SYSTEM
(ONLY THE ENVELOPE IS SHOWN)
(RAD/SEC²) Ω̇
+20
−20
INITIAL CONING ANGLE − 0.25°
FLYWHEEL ACCELERATION
0 1 2 3 496 500 504 508 512 516 520 524 528 532
TIME (SEC)
(RAD/SEC) Ω
4
−4
FLYWHEEL ANGULAR RATE
1/75
(RAD/SEC) ω2
AMPLITUDE SCALE FACTOR
MAGNIFICATION 4 TIMES
BODY ANGULAR RATE
−1/75
1/75
(RAD/SEC) ω3
AMPLITUDE SCALE FACTOR
MAGNIFICATION 4 TIMES
BODY ANGULAR RATE
−1/75

FIGURE 18

with easily available components. The only possible degradation to the system might occur from motor or accelerometer lags. If these lags become troublesome, additional phase compensation can be obtained in the shaping network.

A significant result of the analysis is the required positioning of the accelerometer. In order to obtain control, the flywheel spin axis must be aligned perpendicular to the vehicle spin axis. The accelerometer must be laterally displaced from the vehicle spin axis and in a direction perpendicular to the flywheel axis for stable response. Precise alignment is not necessary and small deviations in alignment can be permitted.

In order to obtain satisfactory response time, the motor-flywheel combination must be capable of delivering a minimum of 200 in-oz of torque, and a speed of 4 radians per second. This will also insure an energy delivery capability large enough to overcome energy losses in the vehicle.

Although it is not necessary to provide active coning damping in the case of one remaining cannister ($R > 1$), the analysis of section 3.1 shows that the system operates satisfactorily in this state. The coning damper may be used to hasten damping action if desired.

SECTION 4

CONING DAMPER USING CONTROL GYROS

4. PRINCIPLE OF OPERATION

An alternate coning-damper design uses single-gimbal gyros in place of the flywheel. Two possible arrangements are shown in Figure 19. A single control gyro is illustrated in Figure 19a. The spin axis nominally coincides with the axis of symmetry of the space vehicle. The gyro is torqued about the space vehicle axis B_2 in accordance with a control law identical to that for the flywheel, except that the control variable is gimbal angle ϕ_2 instead of flywheel speed Ω. The space vehicle angular momentum component along the transverse axis B_3 varies directly with ϕ_2, for small gimbal angles. The lower sketch, Figure 19b, illustrates a two-gyro arrangement. The directions of rotor rotation are opposite, so that no net angular momentum is contributed by the gyros when nulled. Torquing of either or both gyros produces angular momentum changes along the transverse axis B_2. These changes are used for control, in accordance with the coning-damper control law.

4.1 Derivation of the Control-Gyro Equations

Equations of motion of the spinning space vehicle with one or more control gyros are developed from the general equation of rotational motion of a multiple-part body. The version of the general equation used corresponds to the following conditions:

1) No external or body force or torque.

2) Centers of mass of the moving parts (rotors and gimbals) fixed relative to space-vehicle body axes.

3) Origin of space-vehicle body axes at the space-vehicle mass center.

The general equation of motion is (Reference 1, Table 8.4):

$$\begin{aligned} &\mathbf{I}_p \cdot \dot{\boldsymbol{\omega}} + \boldsymbol{\omega} \times \mathbf{I}_p \cdot \boldsymbol{\omega} \\ &+ \sum_{j=1}^{N} \Big[\mathbf{I}_v^j \cdot \dot{\boldsymbol{\omega}} + \mathbf{I}_v^j \cdot \dot{\boldsymbol{\omega}}^j + \dot{\mathbf{I}}_v^j \cdot (\boldsymbol{\omega} + \boldsymbol{\omega}^j) \\ &+ \boldsymbol{\omega} \times (\mathbf{I}_v^j \cdot \boldsymbol{\omega} + \mathbf{I}^j \cdot \boldsymbol{\omega}^j) \Big] = 0 \end{aligned} \qquad (1)$$

TWO CONING-DAMPER ARRANGEMENTS USING SINGLE-GIMBAL CONTROL GYROS

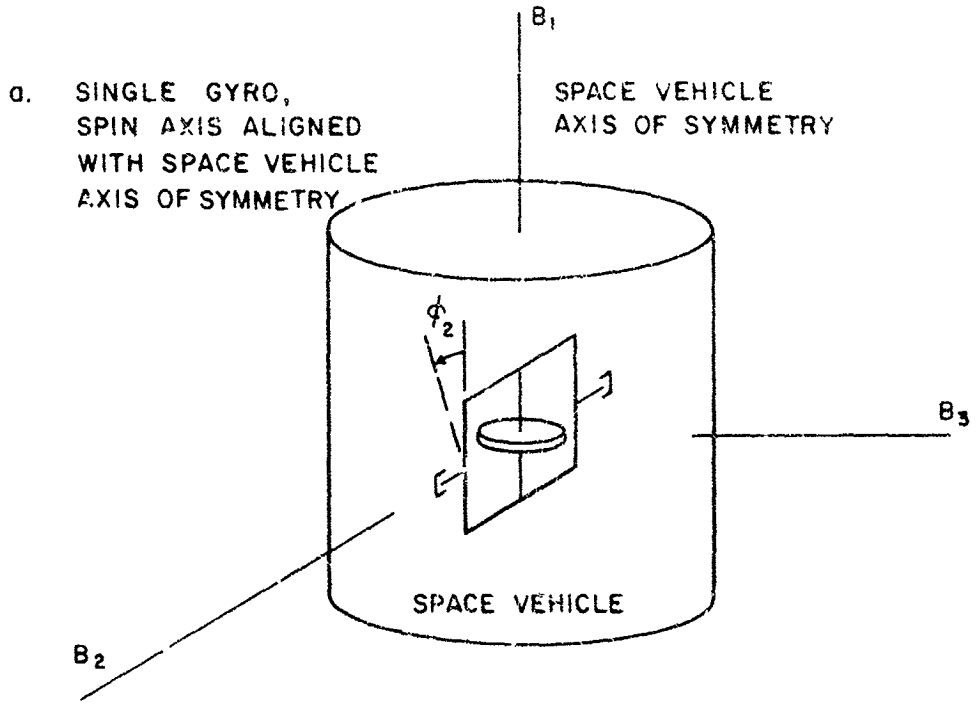

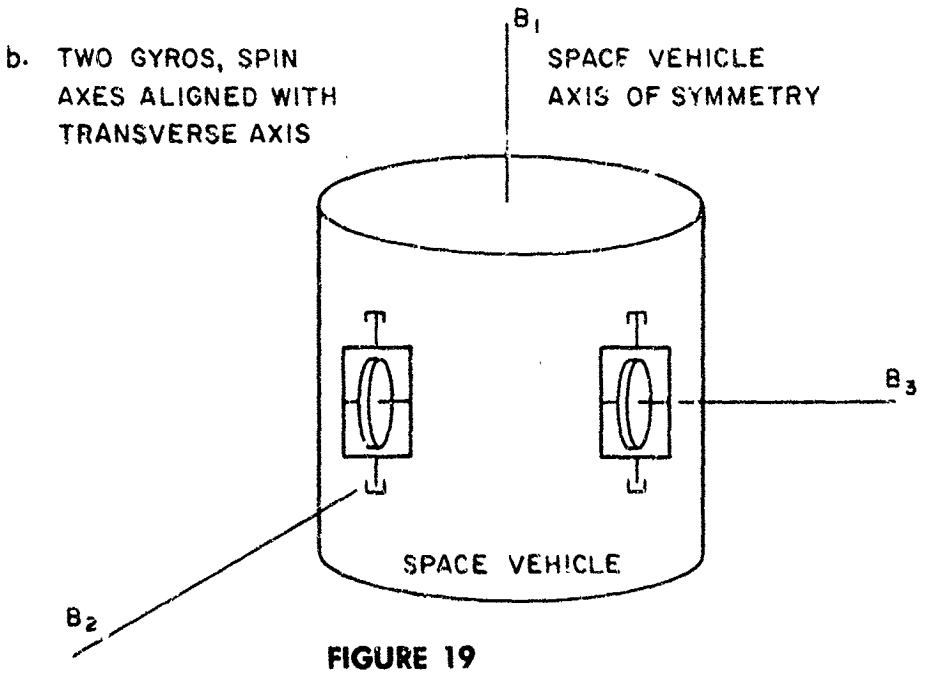

FIGURE 19

ILLUSTRATION OF BODY AXES
FOR ROTOR AND GIMBAL OF GYRO
SHOWN IN FIG. 19 a

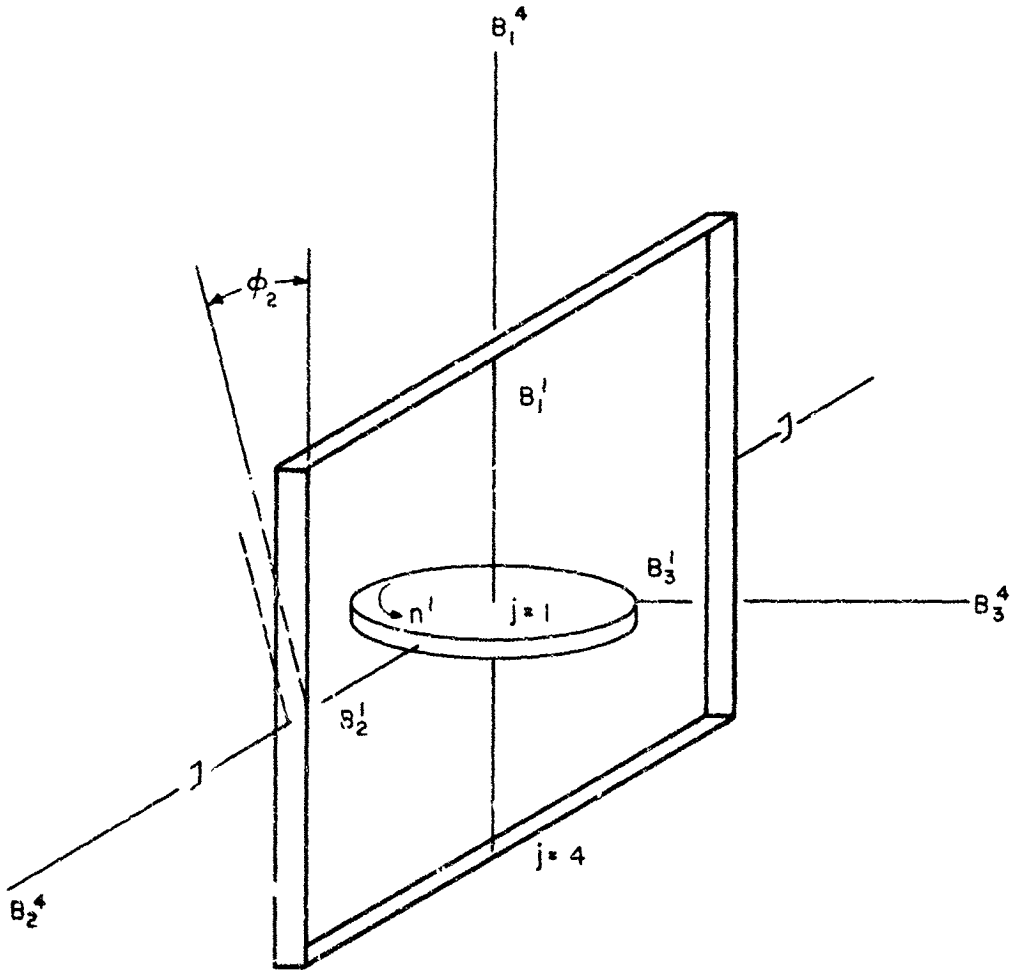

FIGURE 20

The symbols used in this analysis are defined in section 7.1.1 of this section of the report. Following the gyro part-numbering scheme used in the reference, we have:

Space-Vehicle Body Axis Aligned With Gimbal Axis	Rotor Part No.	Gimbal Part No.	
B_1	$j = 3$	$j = 6$	(fig. 19b)
B_2	1	4	(fig. 19a)
B_3	2	5	

The case to be analyzed is the second, illustrated in Figure 19a and Figure 20. The other two cases can be obtained by cyclic permutation of indices over 1, 2, 3, and 4, 5, 6. This must be done for both subscripts and superscripts. The procedure followed in developing scalar equations of motion from Equation (1) is to expand each vector and dyadic into components along space-vehicle body axes. Thus, for the rotor:

$$\mathbf{I}^1 = C^1 \mathbf{b}_1^1 \mathbf{b}_1^1 + A^1 (\mathbf{b}_2^1 \mathbf{b}_2^1 + \mathbf{b}_3^1 \mathbf{b}_3^1) \tag{2}$$

$$= I_{B_1}^1 \mathbf{b}_1 \mathbf{b}_1 + I_{B_2}^1 \mathbf{b}_2 \mathbf{b}_2 + I_{B_3}^1 \mathbf{b}_3 \mathbf{b}_3$$

$$- I_{B_{12}}^1 (\mathbf{b}_1 \mathbf{b}_2 + \mathbf{b}_2 \mathbf{b}_1) - I_{B_{23}}^1 (\mathbf{b}_2 \mathbf{b}_3 + \mathbf{b}_3 \mathbf{b}_2) \tag{3}$$

$$- I_{B_{31}}^1 (\mathbf{b}_3 \mathbf{b}_1 + \mathbf{b}_1 \mathbf{b}_3)$$

The coefficients $I^1_{B_1}$, $I^1_{B_2}$, ..., $I^1_{B_{31}}$ are evaluated in the usual manner by post- and pre- dot multiplying Equation (2) by $\mathbf{b}_1$, $\mathbf{b}_2$, and by pairs of these unit vectors. This gives:

$$I_{B_1}^1 = \mathbf{b}_1 \cdot \mathbf{I}^1 \cdot \mathbf{b}_1 = C^1 (\mathbf{b}_1^1 \cdot \mathbf{b}_1)^2 + A^1 (\mathbf{b}_2^1 \cdot \mathbf{b}_1)^2 = C^1 c^2 \phi_2 + A^1 s^2 \phi_2 \tag{4}$$

$$I_{B_2}^1 = \mathbf{b}_2 \cdot \mathbf{I}^1 \cdot \mathbf{b}_2 = C^1 (\mathbf{b}_1^1 \cdot \mathbf{b}_2)^2 + A^1 (\mathbf{b}_2^1 \cdot \mathbf{b}_2)^2 = A^1 \tag{5}$$

$$I_{B_3^1} = \mathbf{b}_3 \cdot \mathbf{I}^1 \cdot \mathbf{b}_3 = C^1 (\mathbf{b}_1^1 \cdot \mathbf{b}_3)^2 + A^1 (\mathbf{b}_3^1 \cdot \mathbf{b}_3)^2 = C^1 s^2 \phi_2 + A^1 c^2 \phi_2 \tag{6}$$

$$I_{B_{12}^1} = I_{B_{23}^1} = 0 \tag{7}$$

$$I_{B_{31}^1} = -\mathbf{b}_3 \cdot \mathbf{I}^1 \cdot \mathbf{b}_1 = -C^1 (\mathbf{b}_1^1 \cdot \mathbf{b}_3)(\mathbf{b}_1^1 \cdot \mathbf{b}_1) - A^1 (\mathbf{b}_3^1 \cdot \mathbf{b}_3)(\mathbf{b}_3^1 \cdot \mathbf{b}_1) = (C^1 - A^1)\, s\, \phi_2\, c\, \phi_2 \tag{8}$$

Combining these results into Equation (3), we have

$$\begin{aligned} \mathbf{I}^1 = {} & (C^1 c^2 \phi_2 + A^1 s^2 \phi_2)\, \mathbf{b}_1 \mathbf{b}_1 + (C^1 s^2 \phi_2 + A^1 c^2 \phi_2)\, \mathbf{b}_3 \mathbf{b}_3 \\ & + A^1 \mathbf{b}_2 \mathbf{b}_2 + (A^1 - C^1)\, s\, \phi_2\, c\, \phi_2\, (\mathbf{b}_3 \mathbf{b}_1 + \mathbf{b}_1 \mathbf{b}_3) \end{aligned} \tag{9}$$

In a similar manner, we obtain for the gimbal

$$\begin{aligned} \mathbf{I}^4 = {} & (I_1^4 c^2 \phi_2 + I_3^4 s^2 \phi_2)\, \mathbf{b}_1 \mathbf{b}_1 + (I_1^4 s^2 \phi_2 + I_3^4 c^2 \phi_2)\, \mathbf{b}_3 \mathbf{b}_3 \\ & + I_2^4 \mathbf{b}_2 \mathbf{b}_2 + (I_3^4 - I_1^4)\, s\, \phi_2\, c\, \phi_2\, (\mathbf{b}_3 \mathbf{b}_1 + \mathbf{b}_1 \mathbf{b}_3) \end{aligned} \tag{10}$$

The inertia dyadics $\mathbf{I}^1$ and $\mathbf{I}^4$ are partitioned into constant and variable components. The constant components, designated by $\mathbf{I}^1_c$ and $\mathbf{I}^4_c$, are independent of gimbal angle ϕ_2. These components are added to the space-vehicle inertia dyadic components, designated by $\mathbf{I}$, to form a new dyadic:

$$\mathbf{I}_c = \mathbf{I} + \sum_{j=1}^{6} \mathbf{I}_c^j \tag{11}$$

For the gyro under consideration, this is

$$\mathbf{I}_c = \mathbf{I} + \mathbf{I}_c^1 + \mathbf{I}_c^4 = I_1 \mathbf{b}_1 \mathbf{b}_1 + (I_2 + A^1 + I_2^4)\, \mathbf{b}_2 \mathbf{b}_2 + I_3 \mathbf{b}_3 \mathbf{b}_3 \tag{12}$$

In the general case in which the gyro mass centers do not coincide with the origin of space vehicle body axes (the space-vehicle mass center), additional terms are added to $\mathbf{I}_c$ to yield another new dyadic, or

$$\mathbf{I}_p = \mathbf{I}_c + \sum_{j=1}^{N} m^j (\mathbf{r}^j \cdot \mathbf{r}^j \mathbf{E} - \mathbf{r}^j \mathbf{r}^j) \tag{13}$$

The variable portions of $\mathbf{I}^1$ and $\mathbf{I}^4$ are those components which are functions of ϕ_2. These dyadics and their time derivatives, needed for later analysis, are:

$$\mathbf{I}_v^1 = (C^1 c^2 \phi_2 + A^1 s^2 \phi_2)\, \mathbf{b}_1 \mathbf{b}_1 + (C^1 s^2 \phi_2 + A^1 c^2 \phi_2)\, \mathbf{b}_3 \mathbf{b}_3 + (A^1 - C^1)\, s\, \phi_2\, c\, \phi_2\, (\mathbf{b}_3 \mathbf{b}_1 + \mathbf{b}_1 \mathbf{b}_3) \tag{14}$$

$$\dot{\mathbf{I}}_v^1 = (A^1 - C^1)\, \dot{\phi}_2\, s\, 2\, \phi_2\, \mathbf{b}_1 \mathbf{b}_1 + (C^1 - A^1)\, \dot{\phi}_2\, s_2\, \phi_2\, \mathbf{b}_3 \mathbf{b}_3 + (A^1 - C^1)\, \dot{\phi}_2\, c\, 2\, \phi_2\, (\mathbf{b}_3 \mathbf{b}_1 + \mathbf{b}_1 \mathbf{b}_3) \tag{15}$$

$$\mathbf{I}_v^4 = (I_1^4 c^2 \phi_2 + I_3^4 s^2 \phi_2)\, \mathbf{b}_1 \mathbf{b}_1 + (I_1^4 s^2 \phi_2 + I_3^4 c^2 \phi_2)\, \mathbf{b}_3 \mathbf{b}_3 + (I_3^4 - I_1^4)\, s\, \phi_2\, c\, \phi_2\, (\mathbf{b}_3 \mathbf{b}_1 + \mathbf{b}_1 \mathbf{b}_3) \tag{16}$$

$$\dot{\mathbf{I}}_v^4 = (I_3^4 - I_1^4)\, \dot{\phi}_2\, s\, 2\, \phi_2\, \mathbf{b}_1 \mathbf{b}_1 + (I_1^4 - I_3^4)\, \dot{\phi}_2\, s\, 2\, \phi_2\, \mathbf{b}_3 \mathbf{b}_3 + (I_3^4 - I_1^4)\, \dot{\phi}_2\, c\, 2\, \phi_2\, (\mathbf{b}_3 \mathbf{b}_1 + \mathbf{b}_1 \mathbf{b}_3) \tag{17}$$

The angular velocities of the space vehicle and the gyro parts and their derivatives are:

$$\boldsymbol{\omega} = \omega_1 \mathbf{b}_1 + \omega_2 \mathbf{b}_2 + \omega_3 \mathbf{b}_3 \tag{18}$$

$$\dot{\boldsymbol{\omega}} = \dot{\omega}_1 \mathbf{b}_1 + \dot{\omega}_2 \mathbf{b}_2 + \dot{\omega}_3 \mathbf{b}_3 \tag{19}$$

$$\boldsymbol{\omega}^1 = n^1 c\, \phi_2 \mathbf{b}_1 + \dot{\phi}_2 \mathbf{b}_2 - n^1 s\, \phi_2 \mathbf{b}_3 \tag{20}$$

$$\dot{\boldsymbol{\omega}}^1 = -n^1 \dot{\phi}_2\, s\, \phi_2 \mathbf{b}_1 + \ddot{\phi}_2 \mathbf{b}_2 - n^1 \dot{\phi}_2\, c\, \phi_2 \mathbf{b}_3 \tag{21}$$

$$\boldsymbol{\omega}^4 = \dot{\phi}_2 \mathbf{b}_2 \tag{22}$$

$$\dot{\boldsymbol{\omega}}^4 = \ddot{\phi}_2 \mathbf{b}_2 \tag{23}$$

The vector and dyadic components expressed in Equations (9) through (23) are substituted into Equation (1) to yield the desired three scalar equations of rotational motion. This step is routine and tedious, so the final result only is shown here. This is:

$$
\begin{aligned}
&\left[I_{c_1} + (A^1 + I_3^4)\, s^2\, \phi_2 + (C^1 + I_1^4)\, c^2\, \phi_2\right] \dot{\omega}_1 \\
&+ (A^1 - C^1 + I_3^4 - I_1^4)\, s\, \phi_2\, c\, \phi_2\, \dot{\omega}_3 \\
&+ \left[I_{c_3} - I_{c_2} + (A^1 + I_3^4)\, c^2\, \phi_2 + (C^1 + I_1^4)\, s^2\, \phi_2\right] \omega_2\, \omega_3 \\
&+ (A^1 - C^1 + I_3^4 - I_1^4)\, s\, \phi_2\, c\, \phi_2\, \omega_1\, \omega_2 - C^1\, s\, \phi_2\, n^1\, \omega_2 \\
&+ \Big[(A^1 - C^1 + I_3^4 - I_1^4)\, s\, 2\, \phi_2\, \omega_1 + (A^1 - C^1 + I_3^4 - I_1^4)\, c\, 2\, \phi_2\, \omega_3 \\
&\qquad - (A^1 + I_2^4)\, \omega_3 - C^1\, s\, \phi_2\, n^1\Big] \dot{\phi}_2 = 0
\end{aligned}
\tag{24}
$$

$$
\begin{aligned}
&I_{c_2}\, \dot{\omega}_2 + \Big[I_{c_1} - I_{c_3} + (A^1 - C^1 + I_3^4 - I_1^4)\, s^2\, \phi_2 \\
&\qquad + (C^1 - A^1 + I_1^4 - I_3^4)\, c^2\, \phi_2\Big] \omega_3\, \omega_1 \\
&+ (A^1 - C^1 + I_3^4 - I_1^4)\, s\, \phi_2\, c\, \phi_2 \left[(\omega_3)^2 - (\omega_1)^2\right] \\
&+ C^1\, n^1\, (c\, \phi_2\, \omega_3 + s\, \phi_2\, \omega_1) + (A^1 + I_2^4)\, \ddot{\phi}_2 = 0
\end{aligned}
\tag{25}
$$

$$
\begin{aligned}
&\left[I_{c3} + (A^1 + I_3^4)\, c^2 \phi_2 + (C^1 + I_1^4)\, s^2 \phi_2\right] \dot{\omega}_3 \\
&+ (A^1 - C^1 + I_3^4 - I_1^4)\, s\, \phi_2\, c\, \phi_2\, \dot{\omega}_1 \\
&+ \left[I_{c2} - I_{c1} - (C^1 + I_1^4)\, c^2 \phi_2 - (A^1 + I_3^4)\, s^2 \phi_2\right] \omega_1\, \omega_2 \\
&+ (-A^1 + C^1 - I_3^4 + I_1^4)\, s\, \phi_2\, c\, \phi_2\, \omega_2\, \omega_3 - C^1\, c\, \phi_2\, n^1\, \omega_2 \\
&+ \left[(A^1 - C^1 + I_3^4 - I_1^4)\, c\, 2\, \phi_2\, \omega_1 + (-A + C^1 - I_3^4 + I_1^4)\, s\, 2\, \phi_2\, \omega_3\right. \\
&\quad \left. + (A^1 + I_2^4)\, \omega_1 - C^1\, c\, \phi_2\, n^1\right] \dot{\phi}_2 = 0
\end{aligned}
\tag{26}
$$

The following points may be made in reference to Equations (24) to (26):

1) Equations (24) and (26) reduce to the usual Euler equations of rotational motion for a single rigid body in the case where A^1, C^1, and I_i^4, $i = 1,2,3$ are all zero.

2) For the practical case in which the control gyro's mass center is displaced along the B_1 axis by a distance b_1 the I_{c_i}, $i = 1,2,3$ are replaced by I_{p_i}, $i = 1,2,3$, where:

$$
\begin{aligned}
I_{p1} &= I_{c1} \\
I_{p2} &= I_{c2} + (m^1 + m^4)\,(b_1)^2 \\
I_{p3} &= I_{c3} + (m^1 + m^4)\,(b_1)^2
\end{aligned}
\tag{27}
$$

This assumes coincidence of rotor and gimbal mass centers, a reasonable condition.

3) The control torque term is the last term in Equation (26), $-C^1 c\phi_2 n^1 \dot{\phi}_2$. This term dominates all other gyro terms in the equations, for small gimbal angles. All other terms should be neglected for the purpose of initial synthesis.

4) Equations of motion for the space vehicle and other control gyros having gimbal axes aligned with a space-vehicle body axis may be be obtained by cyclic permutation over the indices 1,2,3, and 4,5,6.

4.1.1 Definition of Symbols

A^j, C^j = Diametral and polar moments of inertia for the jth gyro rotor, $j = 1,2,3$

B_i = Space vehicle body axes, $i = 1,2,3$, assumed principal axes for the vehicle less gyros as well as for the composite vehicle.

b_i = Distance component on space vehicle body axes

$\mathbf{b}_i$ = Unit vector on space vehicle body axes

B^j_i = j^{th} moving-part body axes, $i = 1,2,3$, assumed principal axes for the part

$\mathbf{b}^j_i$ = unit vector on j^{th} moving-part body axes, $i = 1,2,3$

c,s = cosine and sine

$\mathbf{E}$ = unit dyadic, or idemfactor

I = moment or product of inertia, with appropriate sub- and superscripts

$\mathbf{I}$ = space vehicle (less gyro rotor and gimbal) inertia dyadic

$\mathbf{I}^j$ = j^{th} moving-part inertia dyadic

$\mathbf{I}^j_c$ = components of the jth moving-part inertia dyadic which have constant values when referred to axes whose origin coincides with the jth moving-part mass center, but which remain aligned with space-vehicle body axes.

$\mathbf{I}^j_v$ = remaining components of the jth moving part inertia dyadic (see previous definition)

$\mathbf{I}_c$ = composite constant-component inertia dyadic, $\mathbf{I}_c = \mathbf{I} + \sum_{j=1}^{N} \mathbf{I}^j_c$

$\mathbf{I}_p$ = sum of the space-vehicle inertia dyadic, the constant parts relative to axes aligned with space-vehicle body axes of the moving-part inertia dyadics, and the moments of inertia of the moving parts considered as point masses located at their respective mass centers (See Equation (13)).

m^j = mass of the jth moving part

N = number of moving parts

n^j = rotor angular velocity relative to space vehicle body axes, assumed constant

$\mathbf{r}^j$ = radius vector of jth moving part from origin of space-vehicle body axes.

ϕ = gimbal angle

$\boldsymbol{\omega}$ = space-vehicle angular velocity, relative to inertial coordinates

$\boldsymbol{\omega}^j$ = angular velocity of the jth moving part relative to space-vehicle body axes.

4.2 Conclusions Regarding the Control-Gyro Coning Damper

The coning-damper design using single-gimbal control gyros in place of the flywheel offers the following advantages relative to the flywheel design:

1) Power Consumption during cyclic operation is determined almost entirely by the power required to keep the rotor spinning at the design speed. Practically no power is required to torque the outer gimbal in accordance with the control law. Although a careful comparison remains to be made, power consumption is expected to be much less than for the flywheel design.

2) Weight of the coning-damper control gyro is expected to be less than for the flywheel. The maximum angular momentum change available for control is given by the rotor angular momentum times the sine of the gimbal angle. This will be larger than the angular momentum change of a flywheel unless maximum speed can be made almost as large as that of a gyro rotor (about 10,000 rpm).

Disadvantages of the single gimbal gyro relative to the flywheel for the coning-damper application are:

1) Analytical complexity results from the complicated form of the equations of motion of a space vehicle and single-gimbal gyro. These equations are developed in 3.0 of this section of the report.

2) Cross-coupling effects may be significantly large unless gimbal angles are limited to small values. This can be established only by a detailed analysis.

3) Off-the-shelf components unsuitable - The angular momentum delivery capabilities of a standard HIG type gyro may be inadequate. This is about 0.005 slug-ft^2/sec for a gimbal angle of 7 degrees. A value of about 0.1 slug-ft^2/sec is needed, based on tentative sizing.

4) Cost is expected to be greater than for the flywheel.

SECTION 5

GENERAL CONCLUSIONS

5. RESULTS

From the results of the analysis of the external torques and the analysis of the control system, the concept of spacecraft attitude stabilization by coning damping action has been demonstrated to be feasible as well as practical. The results of Section 2 indicate the effects of gravitational and magnetic field interactions with the vehicle are very small. The tip-off incurred by the cannister separation mechanisms has been shown to be a maximum of $0.136^{\circ}(3\sigma)$ which is well within the mission accuracy requirements.

The analysis of the coning damper control system in Section 3 has shown that relatively simple, low performance control components will suffice. A single system can provide coning damping for the three spacecraft configurations, both before and after the cannisters are successively ejected. The chosen system consists of an accelerometer for sensing coning motion and a motor-flywheel as a momentum device. The required characteristics of this equipment can be achieved with existing proven components. The expected positioning and alignment errors in mounting these components have been shown to have little or no effect on system operation. In order to achieve the desired flywheel torque speed characteristic, a relatively small, low power motor may be used.

An alternate approach of mechanization of the coning damper is given, using a control gyro. This is expected to be a more efficient energy transfer device than the flywheel system. However, the cost of the alternate system is expected to exceed the simpler flywheel system.

BIBLIOGRAPHY

1. Abzug, Malcolm J., Active Satellite Attitude Control. Douglas Aircraft Company Engineering Paper No. 1218. August, 1961.

2. Douglas Report No. SM-41393, An Electromechanical Coning Damper Rebound Project. January, 1962.

APPENDIX I

SYSTEM EQUATIONS FOR THE CONING DAMPER USING A MOTOR-FLYWHEEL

The following is a derivation in body coordinates of the equations of motion for a spin-stabilized satellite, with dynamic symmetry along an axis (letting both the control wheel and the accelerometer be perfectly positioned and oriented as is shown in Figure 6), followed by a summary of formulae for various properties of the solution. The latter is facilitated by tailoring the autopilot gain so as to eliminate undesirable terms from the accelerometer, thus resulting in an optimum value for this parameter (large variations in this value can be tolerated, however, and would in fact be used). The notation used is given immediately below.

A	Constant $= \frac{-I_P}{I_1 r_3} = \frac{\kappa_1 \kappa_m}{r_m}$
B	Constant $= \frac{1}{r_m}$
F	Coning damper theoretical efficiency, equation 29
h	Constant $= \frac{I_P}{I_1}\left(2 - \frac{I_R}{I_P}\right) r_m$
H	Magnitude of angular momentum
I_P	Pitch-yaw moment of inertia for the total vehicle
I_1	Roll moment of inertia for the control wheel
I_R	Roll moment of inertia for the total vehicle
κ_1	Accelerometer gain
κ_m	Motor gain
λ	Constant $\left(1 - \frac{I_R}{I_P}\right)$
$\frac{1}{\mu}$	Time constant for the coning angle time history, equation 18

c	Initial condition $\left[\omega_2(0) = -c\right]$
p	Laplace variable
r_1	Displacement of accelerometer along center line
s	Initial vehicle spin rate
r_3	Distance of accelerometer from the center line
τ_m	Motor time constant
ω_1	Roll rate of the vehicle (seen in body)
ω_2	Pitch rate of the vehicle (seen in body)
ω_3	Yaw rate of the vehicle (seen in body)
Ω	Spin of the wheel relative to main body
θ	Coning angle

The generalized Euler equations for the two interacting parts are

(1) $$\dot{\omega}_1 - \frac{I_1}{I_R}\omega_3 = 0$$

(2) $$\dot{\omega}_2 - \left(1 - \frac{I_R}{I_P}\right)\omega_1\omega_3 + \frac{I_1}{I_P}\dot{\Omega} = 0$$

(3) $$\dot{\omega}_3 + \left(1 - \frac{I_R}{I_P}\right)\omega_2\omega_3 + \omega_1\frac{I_1}{I_P}\Omega = 0$$

The coning angle at any one time is

(4) $$\theta = \cos^{-1}\left(\frac{I_R\omega_1}{H}\right)$$

and its rate of change is obtained by the use of (1)

(5) $$-\sin\theta\,\dot{\theta} = \frac{I_1\omega_3}{H}\Omega$$

If Ω could be made proportional to ω_3 by choosing a positive proportionality factor, then $\dot{\theta}$ would always be negative (except at those times when $\omega_3 = 0$).

This linearity can be achieved by aligning the accelerometer as in Figure 6. With such an alignment the accelerometer reading is:

(6) $$a_1 = \left\{ r_3(\dot{\omega}_2 + \omega_3\omega_1) - r_1(\omega_2^2 + \omega_3^2) \right\}$$

which is obtained from an expansion of the general acceleration equation

(7) $$\vec{a} = \dot{\vec{\omega}} \times \vec{r} + \vec{\omega} \times (\vec{\omega} \times \vec{r})$$

The second term of a_1 is constant for a rigid body undergoing no energy changes but for this situation it decreases exponentially with a large time constant as the coning is reduced with the damper.

The motor amplifier combination can be represented by the following transfer function (no torque limiting)

(8) $$\frac{\Omega}{a_1} = \frac{K_1 K_m}{1 + \tau_m s}$$

If no other control is used equation (8) can be arranged in the following form for the control equation

(9) $$\dot{\Omega} = Aa_1 - B\Omega$$

If (2) and (6) are substituted in (9) the relation for A (independent of B) is

(10) $$A = -\frac{I_P}{I_1 r_3}$$

where the d.c. term in (6) has been taken out with a filter. This allows Ω to become

(11) $$\Omega = \left(\frac{2I_P - I_R}{I_1 B}\right)\omega_1\omega_3$$

or

(12) $$\Omega = h\omega_1\omega_3$$

which is the expression desired for control, as deduced from (5). This establishes the control capability using a motor and d-c filter, with the accelerometer properly placed.

It is of interest to know the damping rate of the control system. This is derived as follows.

From (1) the two relations $\left[\text{where } s = \omega_1(0)\right]$

(13) $$\frac{\dot{\omega}_1}{\omega_1} = \frac{i_1 h}{I_R}\omega_3^2$$

(14) $$\omega_1 = s\, e^{\frac{i_1 h}{I_R}\int \omega_3^2\, dt}$$

Starting with equation (12) and substituting in (3), (2), (1), (13), (14), in order, results in the following exact but nonlinear expression for the system characteristic equation

(15) $$\ddot{\omega}_3 + 2\mu\lambda\dot{\omega}_3 + \lambda^2\omega_3 = 0$$

with μ and λ defined as

(16) $$2\mu\lambda = \frac{I_1 I_R}{I_P^2} h s^2 e^{\frac{2 i_1 h}{I_R}\int \omega_3^2\, dt}\left(1 - \frac{I_P^2\,\omega_3^2}{I_R^2\,\omega_1^2}\right)$$

(17) $$\lambda^2 = \left[1 - \frac{I_R}{I_P}\, s\, e^{\frac{I_1 h}{I_R}\int \omega_3^2\, dt}\right]^2\left[1 + \frac{I_1^2\, h^2\,\omega_3^2}{I_P - I_R{}^2}\right]$$

The exponentials can be considered unity for small angles of coning. For the parameters being used (16) and (17) can be approximated by

(18) $$\mu = \frac{1}{2}\left[\frac{I_R}{I_P}\,\frac{\left(2 - \frac{I_R}{I_P}\right)}{\left(1 - \frac{I_R}{I_P}\right)}\right]\frac{s}{B}$$

(19) $$\lambda = \left(1 - \frac{I_R}{I_P}\right) s$$

which form the damping rate and undamped natural frequency, respectively. The damped natural frequency will then be

(20) $$\beta = \sqrt{1 - \mu^2}\,\lambda$$

and for initial conditions of $\omega_2(0) = -c$, $\omega_3(0) = 0$ the time history for ω_3 is

(21) $$\omega_3 = c\, e^{-\mu\lambda t}\sin\beta t$$

The efficiency of the control system is also an important factor; efficiency is here defined as the ratio of the energy imparted to the vehicle structure to that drawn from a storage battery into a perfect motor. For a body of revolution the rate of change of rotational energy is

$$(22) \qquad \dot{E} = -\frac{H^2}{2I_R}\left(1 - \frac{I_R}{I_P}\right)\sin 2\theta\,\dot{\theta}$$

so that after manipulation of (4), (5), (1), and (12) the following is obtained

$$(23) \qquad \dot{E} = I_1 h \left(1 - \frac{I_R}{I_P}\right) s^2 \omega_3^2 \; .$$

the power (W) supplied to an ideal motor, since the vehicle is large compared to the wheel, is approximately

$$(24) \qquad W = (I_1 \dot{\Omega})\,\Omega$$

where in this application the approximation is very accurate Manipulation of (12), (13) and (14) yields

$$(25) \qquad \dot{\Omega} = hs\, e^{\frac{I_1 h}{I_R}\int \omega_3^2\, dt} \left(\frac{I_1 h}{I_R}\omega_3^2 + \dot{\omega}_3\right) .$$

so that, again letting the spin be constant in (12) and (25) the following is obtained from (21) for the two expressions (23) and (24) respectively

$$(26) \qquad \dot{E} = I_1 h \left(1 - \frac{I_R}{I_P}\right) s^2 c^2 \left[e^{-2\mu t} \sin^2 \beta t \right]$$

$$(27) \qquad W = I_1 h^2 s^2 c^2 \left[\frac{I_1 h c^2}{I_R} e^{-4\mu t} \cos^4 \beta t - e^{-2\mu t} (\mu \sin^{-2} \beta t - 1/2\, \beta \sin^2 \beta t) \right]$$

The work efficiency is defined in view of the practical restrictions on the electrical equipment. Energy must be drawn from a storage battery to accelerate the wheel during the first quarter cycle. During the second quarter cycle or deceleration phase energy cannot be returned to the battery, but no energy must be drawn from it. The theoretical work efficiency therefore is the work done on

the structure during the first half cycle divided by the work done on the motor during the first quarter cycle.

$$(28) \qquad \langle F \rangle = \frac{\int_0^{\frac{\pi}{2\beta}} \dot{E}\, dt}{\int_0^{\frac{\pi}{4\beta}} W\, dt}$$

or

$$(29) \qquad \langle F \rangle \approx \pi \frac{l_1}{l_p} \left[\frac{B}{s} \left(\frac{1}{2 - \frac{l_R}{l_p}} \right) \right]$$

APPENDIX II

MATHEMATICAL ANALYSIS OF THE EXTERNAL DISTURBANCES ON A SPIN-STABILIZED VEHICLE

The generalized equations of motion for a spinning vehicle acted upon by external torques which may be a function of the position in orbit will now be derived. A list of symbols used is given first as follows:

a	Magnetic constant for the earth $\left(2.0 \times 10^{16} \frac{\text{lbs-ft}^2}{\text{amp}}\right)$
α	Constant $= \frac{I_R}{I_P} s$
α_i $(i=1,2,3)$	Direction cosines of local vertical as seen in body
$\vec{B}$	Magnetic induction vector
B_i $(i=1,2,3)$	Inertial components of magnetic induction
β	Mean anomaly rate
δ_g	Angular displacement (magnitude) due to gravitational field of the momentum vector
δ_m	Angular displacement (magnitude) due to magnetic field of the momentum vector
$\hat{\vec{e}}$	Unit vector along local vertical
C	Constant, equation 27
$\hat{\vec{\gamma}}$	Vector normal to both the symmetry axis and local vertical having the same sense as gravitational torque
$\mathbf{I}$	Moment of inertia dyadic
I_P	Pitch-yaw moment of inertia
I_R	Roll moment of inertia
λ	Constant, equation 31
M	Constant $= -\frac{M}{I_P}\left(\frac{a}{r^3}\right)$

m	Magnitude of spacecraft magnetic dipole moment
$\vec{m}$	Spacecraft magnetic dipole moment vector
μ	Gravitational constant for the earth $1.4 \times 10^{16} \frac{ft^2}{sec^2}$
$\hat{\vec{n}}$	Unit vector along earth's magnetic axis
$\vec{p}$	Moment of momentum
ϕ	Angle between orbit axis and earth axis
Q_i $(i=1,2,3)$	Generalized torque along axis of rotation for q_i
Q_i^g $(i=1,2,3)$	Generalized gravitational torque
Q_i^m $(i=1,2,3)$	Generalized magnetic torque
q_i $(i=1,2,3)$	Euler angle used as generalized coordinates
R	Orbital radius
S	Spacecraft spin
T	Rotational kinetic energy
t	Real time
$\vec{r}_g$	Torque due to gravitational field
$\vec{r}_m$	Torque due to magnetic field
$\vec{r}_s$	Torque due to solar radiation (negligible)
θ	Angle between vehicle symmetry axis and local vertical
V	Potential function for gravity torque
ν	Speed in orbit
$\vec{\omega}$	Spacecraft angular velocity
ω_i $(i=1,2,3)$	Body components of angular velocity
$\vec{\Omega}$	Orbital angular velocity
x	Complex representation of angular displacement of the spacecraft center-line

X_i $(i=1,2,3)$	Space-fixed coordinate system S
X'_i $(i=1,2,3)$	Body-fixed coordinate system S'
ξ_i $(i=1,2)$	Inertial components of angular displacement of the spacecraft center-line
ξ^*_i $(i=1,2)$	Inertial components of angular displacement of the spacecraft moment of momentum

THE GENERAL EQUATIONS OF MOTION

In body reference

(1) $$\frac{d\vec{p}}{dt} + \vec{\omega} \times \vec{p} = \vec{r}_g + \vec{r}_m + \vec{r}_s$$

(2) $$\vec{p} = \mathbf{I} \cdot \vec{\omega}$$

(3) $$\frac{d\mathbf{I}}{dt} = 0$$

where $\vec{r}_g, \vec{r}_m$ and $\vec{r}_s$ are defined below and as such complete the description

(4) $$\vec{r}_g = \frac{3\mu}{R^3}\left[\hat{\vec{e}} \times (\mathbf{I} \cdot \hat{\vec{e}})\right]$$

(5) $$\vec{r}_m = \vec{m} \times \vec{B}$$

(6) $$\vec{r}_s = \vec{o}$$

(7) $$\vec{B} = -\frac{a}{R^3}\left[\hat{\vec{n}} - \hat{\vec{e}}\,(\hat{\vec{n}} \cdot \hat{\vec{e}})\right]$$

(8) $$\frac{d\vec{m}}{dt} = \vec{o}$$

(9) $$\frac{d\hat{\vec{e}}}{dt} + (\vec{\omega} - \vec{\Omega}) \times \hat{\vec{e}} = \vec{o}$$

(10) $$\frac{d\hat{\vec{n}}}{dt} + \vec{\omega} \times \hat{\vec{n}} = \vec{o}$$

For the purpose of writing Hamilton's equation in terms of the Euler angles q_1, q_2, q_3 (Figure 21) the components of both $\vec{r}_g, \vec{r}_m$ are evaluated along the respective axes of instantaneous rotation.

COORDINATE SYSTEMS FOR EXTERNAL TORQUES

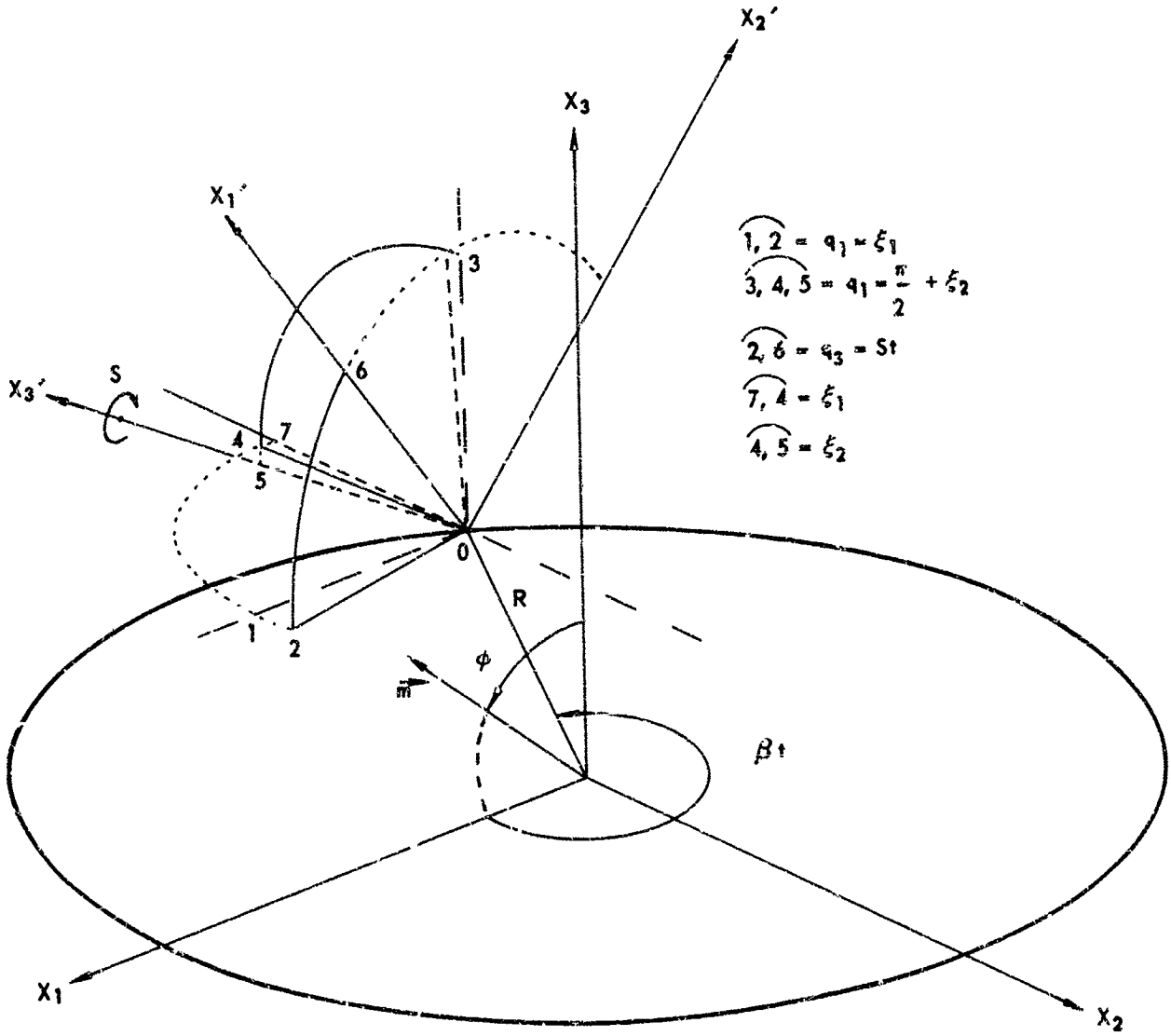

$S = (X_1, X_2, X_3)$ FIXED IN SPACE

$S' = (X_1', X_2', X_3')$ FIXED IN BODY

FIGURE 21

The form of $\vec{r}_m$ in space, with $\vec{B} = \begin{pmatrix} B_1 \\ B_2 \\ B_3 \end{pmatrix}$ is (since $\vec{m}$, the spacecraft magnetic dipole, is parallel to the axis of symmetry)

$$(11) \quad r_m = m \begin{pmatrix} B_3 \cos q_1 \sin q_2 - B_2 \cos q_2 \\ B_1 \cos q_2 - B_3 \sin q_1 \sin q_2 \\ B_2 \sin q_1 \sin q_2 + B_1 \cos q_1 \sin q_2 \end{pmatrix}$$

and resolved along the space 3-axis (for q_1), the line of nodes (for q_2) and the body 3-axis (for q_3)

$$(12a) \quad Q_1^m = m\,(B_1 \cos q_1 \sin q_2 + B_2 \sin q_1 \sin q_2)$$

$$(12b) \quad Q_2^m = m\,(B_1 \sin q_1 \cos q_2 - B_2 \cos q_1 \cos q_2 - B_3 \sin q_2)$$

$$(12c) \quad Q_3^m = 0$$

The form of $\vec{r}_g$ in the vehicle is

$$(13) \quad \vec{r}_g = \frac{3\mu}{R^3} I_P \left[1 - \frac{I_R}{I_P}\right] \begin{pmatrix} -\alpha_2 \\ \alpha_1 \\ 0 \end{pmatrix} \alpha_3$$

where if $\hat{\vec{e}}$ is written in the body as

$$(14) \quad \hat{\vec{e}} = \begin{pmatrix} \alpha_1 \\ \alpha_2 \\ \alpha_3 \end{pmatrix}$$

so that the angle θ between $\vec{e}$ and the body 3-axis is

$$(15) \quad \cos\theta = \begin{pmatrix} 0 \\ 0 \\ 1 \end{pmatrix} \cdot \begin{pmatrix} \alpha_1 \\ \alpha_2 \\ \alpha_3 \end{pmatrix} = \alpha_3$$

while the vector $\vec{\gamma}$ normal to the plane formed by the two previous lines is

(16) $$\vec{\gamma} = \begin{pmatrix} 0 \\ 0 \\ 1 \end{pmatrix} \times \begin{pmatrix} a_1 \\ a_2 \\ a_3 \end{pmatrix} = \begin{pmatrix} -a_2 \\ a_1 \\ 0 \end{pmatrix} = \hat{\vec{\gamma}} \sin\theta$$

then the expression for $\vec{r}_g$ becomes

(17) $$\vec{r}_g = \frac{3\mu}{R^3} \hat{\vec{\gamma}}\, l_P \left(1 - \frac{l_R}{l_P}\right. \sin\theta \cos\theta$$

and in terms of the potential $V = G \cos^2\theta$

(18) $$\vec{r}_g = \left(-\frac{\partial V}{\partial \theta}\right) \hat{\vec{\gamma}}$$

thus writing V as a function of q_1, q_2, q_3

(19) $$V = G \sin^2 (q_1 - \beta t) \sin^2 q_2$$

obtain $Q_i^g = -\dfrac{\partial V}{\partial q_i}$

(20a) $$Q_1^g = -G \sin 2 (q_1 - \beta t) \sin^2 q_2$$

(20b) $$Q_2^g = -G \sin^2 (q_1 - \beta t) \sin 2q_2$$

(20c) $$Q_3^g = 0$$

Hamilton's equation for the generalized momenta p_i are $(i = 1,2,3)$

(21) $$\frac{dp_i}{dt} = -\frac{\partial T}{\partial q_i} + Q_i$$

where

(22) $$p_i = \frac{\partial T}{\partial \dot{q}_i}$$

with T, the kinetic energy, given by

$$(23)\quad T = \frac{1}{2} I_P (\omega_1^2 + \omega_2^2) + \frac{1}{2} I_R \omega_3^2 = \frac{1}{2} \left[I_P (\dot{q}_2^2 + \dot{q}_1^2 \sin^2 q_2) + I_R (\dot{q}_3 + \dot{q}_1 \cos q_2)^2 \right]$$

so that both

$$(24a)\quad p_1 = (I_P \sin^2 q_2 + I_3 \cos^2 q_2)\, \dot{q}_1 + I_R\, \dot{q}_3 \cos q_2$$

$$(24b)\quad p_2 = I_P\, \dot{q}_2$$

$$(24c)\quad p_3 = I_R (\dot{q}_3 + \dot{q}_1 \cos q_2)$$

and

$$(25a)\quad \dot{p}_1 = - G \sin 2 (q_1 - \beta t) \sin^2 q_2 + m [B_1 \cos q_1 \sin q_2 + B_2 \sin q_1 \sin q_2]$$

$$(25b)\quad \dot{p}_2 = - G \sin^2 (q_1 - \beta t) \sin 2 q_2 + m [B_1 \sin q_1 \cos q_2 - B_2 \cos q_1 \cos q_2 - B_3 \sin q_2]$$
$$- I_P\, \dot{q}_1^2 \sin q_2 \cos q_2 - I_R (\dot{q}_3 + \dot{q}_1 \cos q_2)\, \dot{q}_2 \sin q_2$$

$$(25c)\quad \dot{p}_3 = 0$$

If one makes the transformations $q_1 = \xi_1 \quad q_2 = \frac{\pi}{2} + \xi_2 \quad q_3 = St$ then assumes ξ_1, ξ_2 to be small and S = const (S is the spin) there results the following two equations.

$$(26a)\quad \ddot{\xi}_1 - \frac{I_R}{I_P} S \dot{\xi}_2 + \left(\frac{2G}{I_P} \cos 2\beta t - m \frac{B_2}{I_P} \right) \xi_1 = \frac{G}{I_P} \sin 2\beta t + m \frac{B_1}{I_1}$$

$$(26b)\quad \ddot{\xi}_2 + \frac{I_R}{I_P} S \dot{\xi}_2 + \left(\frac{2G}{I_P} \sin^2 \beta t - m \frac{B_2}{I_P} \right) \xi_2 = - m \frac{B_3}{I_P}$$

From (17,18) G is

$$(27) \qquad G = \frac{3}{2}\,\frac{\mu}{R^3}\, I_P\left(1 - \frac{I_R}{I_P}\right)$$

and if the speed in orbit is $\nu = R\beta$ (for circular orbit)

$$(28) \qquad \nu^2 = \frac{\mu}{R}$$

then

$$(29) \qquad \frac{\mu}{R^3} = \beta^2$$

or

$$(30) \qquad \frac{G}{I_P} = \frac{3}{2}\,\lambda^2$$

with

$$(31) \qquad \lambda = \sqrt{1 - \frac{I_R}{I_P}}\,\beta$$

Let the orbit make an angle ϕ with the equator so that $\vec{B}$ looks in space (equation 7) as follows

$$(32) \qquad \vec{B} = -\frac{a}{R^3}\begin{pmatrix} \sin\phi\,(1 - 3\cos^2\beta t) \\ -\frac{3}{2}\sin\phi\,\sin 2\beta t \\ \cos\phi \end{pmatrix}$$

having chosen $\hat{\vec{n}}$ to be in the space 1 - 3 plane and $\hat{\vec{e}}$ along the 1-axis at t=o

$$(33) \qquad \hat{\vec{n}} = \begin{pmatrix} \sin\phi \\ 0 \\ \cos\phi \end{pmatrix}$$

(34) $$\hat{\vec{e}} = \begin{pmatrix} \cos \beta t \\ \sin \beta t \\ 0 \end{pmatrix}$$

The final form of the equation is then, for $M = -\frac{m}{I_p}\frac{a}{R^3}$

(35a) $$\ddot{\xi}_1 - \frac{I_R}{I_p} S \dot{\xi}_2 + [3\lambda^2 \cos 2\beta t + \frac{3}{2} M \sin\phi \sin 2\beta t]\, \xi_1 = \frac{3}{2}\lambda^2 \sin 2\beta t + M \sin\phi\,(1 - 3\cos^2 \beta t)$$

(35b) $$\ddot{\xi}_2 + \frac{I_R}{I_p} S \dot{\xi}_1 + [-3\lambda^2 \sin^2 \beta t + \frac{3}{2} M \sin\phi \sin 2\beta t]\, \xi_2 = -M \cos\phi$$

SOLUTIONS

A. Gravitational Field Effect

The linearized equations in this case are just

(36a) $$\ddot{\xi}_1 - \frac{I_R}{I_p} S \dot{\xi}_2 + 3\lambda^2 \xi_1 \cos 2\beta t = \frac{3}{2}\lambda^2 \sin 2\beta t$$

(36b) $$\ddot{\xi}_2 + \frac{I_R}{I_p} S \dot{\xi}_1 - 3\lambda^2 \xi_2 \sin^2 \beta t = 0$$

Define $x = \xi_1 + i\,\xi_2$ and let $\alpha = \frac{I_R}{I_p} S$, then

(37) $$\ddot{x} + i\,\alpha\,\dot{x} + 3\lambda^2 x \cos 2\beta t = \frac{3}{2}\lambda^2 \sin 2\beta t - 3\lambda^2 \xi_2 \cos^2 \beta t$$

The above looks like a Matheiu equation with a driving function except for the expression involving ξ_2. If $|x| << 1$ then the term in x (also that in ξ_2) can be neglected relative to the right hand side while λ is already small compared to α. For later application this turns out to be the case so the following assumes it

(38) $\ddot{x} + i\alpha\dot{x} = \frac{3}{2}\lambda^2 \sin 2\beta t$

but $\sin 2\beta t = -\frac{1}{2} i \left(e^{2i\beta t} - e^{-2i\beta t}\right)$ or

(39) $\ddot{x} + i\alpha\dot{x} = -\frac{3}{4} i \lambda^2 \left(e^{2i\beta t} - e^{-2i\beta t}\right)$

Integrating once

(40) $\dot{x} = e^{-i\alpha t} \int -\frac{3}{4} i \lambda^2 \left(e^{2i\beta t} - e^{-2i\beta t}\right) e^{i\alpha t}\, dt$

$$= -\frac{3}{4}\lambda^2 \left(\frac{e^{2i-t}}{\alpha + 2\beta} - \frac{e^{-2i\beta t}}{\alpha - 2\beta}\right) + C_2 e^{-i\alpha t}$$

so if the initial condition is

(41) $C_2 = -3\left(\frac{\beta\lambda^2}{\alpha^2 - 4\beta^2}\right)$

Integrating again

(42) $x = \frac{3}{8} i \frac{\lambda^2}{\beta}\left(\frac{e^{2i\beta t}}{\alpha + 2\beta} + \frac{e^{-2i\beta t}}{\alpha - 2\beta}\right) + \frac{i}{\alpha} C_2 e^{-i\alpha t} + C_1$

and if the initial condition is $x(o) = o$

(43) $C_1 = -\frac{3}{4} i \frac{\lambda^2}{\alpha\beta}\left(\frac{1}{\alpha^2 - 4\beta^2}\right)$

The component form of the equation in x is thus

(44a) $\xi_1 = \frac{\lambda^2}{\alpha^2 - 4\beta^2}\left[\frac{3}{2}\sin 2\beta t - 3\frac{\beta}{\alpha}\sin \alpha t\right]$

(44b) $$\xi_2 = \frac{\lambda^2}{\alpha^2 - 4\beta^2}\left[\frac{3}{4}\,\frac{\alpha}{\beta}\,(\cos 2\beta t - 1) + 3\,\frac{\beta}{\alpha}\,(\cos \alpha t - 1)\right]$$

B. Magnetic Field Effect

The linearized equations in this case are just

(45a) $$\ddot{\xi}_1 - \frac{I_R}{I_P}\,S\,\dot{\xi}_2 + \frac{3}{2}\,M\,\xi_1 \sin\phi \sin 2\beta t = M \sin\phi\,(1 - 3\cos^2 \beta t)$$

(45b) $$\ddot{\xi}_2 + \frac{I_R}{I_P}\,S\,\dot{\xi}_1 + \frac{3}{2}\,M\,\xi_2 \sin\phi \sin 2\beta t = -\,M \cos\phi$$

Define as before $x = \xi_1 + i\,\xi_2$ and $\alpha = \frac{I_R}{I_P}\,S$, then

(46) $$\ddot{x} + i\,\alpha\,\dot{x} + \frac{3}{2}\,M\,x \sin\phi \sin 2\beta t = M\,[\sin\phi\,(1 - 3\cos^2 \beta t) - i\cos\phi]$$

The above is a modified Matheiu equation with a driving function. If, once again, $|x| << 1$ then the term in x can be neglected relative to the right hand side while M is assumed small relative to α . For later application this is justified so making such an assumption there results

(47) $$\ddot{x} + i\,\alpha\,\dot{x} = M\,[\sin\phi\,(1 - 3\cos^2 \beta t) - i\cos\phi]$$

but $$1 - 3\cos^2 \beta t = -\,\frac{1}{4}\left[2 + 3\,(e^{2i\beta t} + e^{-\,2i\beta t})\right]$$ or

(48) $$\ddot{x} + i\,\alpha\,\dot{x} = -\,M\left[\frac{3}{4}\,(e^{2i\beta t} + e^{-\,2i\beta t}) \sin\phi + \frac{1}{2}\,(\sin\phi + 2i\cos\phi)\right]$$

Integrating once

(49) $$\dot{x} = e^{-\,i\alpha t}\int -\,M\,e^{i\alpha t}\left[\frac{3}{4}\,(e^{2i\beta t} + e^{-\,2i\beta t}) \sin\phi + \frac{1}{2}\,(\sin\phi + 2i\cos\phi)\right]dt$$

$$= M\left[\frac{3}{4}\,i\,\frac{e^{2i\beta t}}{\alpha + 2\beta} + \frac{e^{-\,2i\beta t}}{\alpha - 2\beta}\,\sin\phi + \frac{1}{\alpha}\,(-\cos\phi + \frac{i}{2}\sin\phi)\right] + C_2\,e^{i\alpha t}$$

so if the initial condition is $\dot{x}(o) = o$

$$(50) \quad C_2 = \frac{M}{\alpha} \left[\cos\phi - 2i \frac{\alpha^2 - \beta^2}{\alpha^2 - 4\beta^2} \sin\phi\right]$$

Integrating again

$$(51) \quad x = M\left[\frac{3}{8\beta}\left(\frac{e^{2i\beta t}}{\alpha + 2\beta} - \frac{e^{-2i\beta t}}{\alpha - 2\beta}\right)\sin\phi - \frac{1}{\alpha}\left(\cos\phi - \frac{1}{2} i \sin\phi\right) t\right] + C_2 e^{i\alpha t} + C_1$$

and if the initial condition is $x(o) = o$

$$(52) \quad C_1 = -\frac{M}{\alpha^2}\left(\frac{1}{2}\sin\phi + i\cos\phi\right)$$

The component form of the equation in x is thus

$$(53a) \quad \xi_1 = M\left[-\frac{3}{2}\left(\frac{1}{\alpha^2 - 4\beta^2}\right)\sin\phi\cos 2\beta t + \frac{2}{\alpha^2}\left(\frac{\alpha^2 - \beta^2}{\alpha^2 - 4\beta^2}\right)\sin\phi\cos\alpha t\right.$$
$$\left. + \frac{1}{\alpha^2}\cos\phi\sin\alpha t + \frac{1}{\alpha} t\cos\phi - \frac{1}{2\alpha^2}\sin\phi\right]$$

$$(53b) \quad \xi_2 = M\left[\frac{3}{4}\frac{\alpha}{\beta}\left(\frac{1}{\alpha^2 - 4\beta^2}\right)\sin\phi\sin 2\beta t - \frac{2}{\alpha^2}\left(\frac{\alpha^2 - \beta^2}{\alpha^2 - 4\beta^2}\right)\sin\phi\sin\alpha t\right.$$
$$\left. + \frac{1}{\alpha^2}\cos\phi\cos\alpha t + \frac{1}{2\alpha} t\sin\phi - \frac{1}{\alpha^2}\cos\phi\right]$$

APPLICATION TO REBOUND

Equation (45 a, b) and (53 a, b) give the angular motion of the spacecraft centerline and not that of the moment of momentum. A comparison of the vehicle and orbit parameters shows that the dominant coefficients in these equations are exactly those associated with the low, or orbital, frequency terms and as such describe the average angular motion of the moment of momentum since these terms overwhelm in magnitude the frequencies related to the spin. The form of the angular motion of the moment of momentum is now given for the two field cases in the order,

gravitational and magnetic

(54a) $\xi_1^* = 0$

(54b) $\xi_2^* = A_0 (\cos 2\beta t - 1)$

(55a) $\xi_1^* = A_1 t$

(55b) $\xi_2^* = A_2 t + B \sin 2\beta t$

The magnitude of the deviation for either effect is

(55) $$\delta = \sqrt{\xi_1^{*2} + \xi_2^{*2}}$$

and appears in this form in section 2